

hep-ph/0105089
ROMA1-TH/2001-1313

The 2+2 and 3+1 Four-Family Neutrino Mixing at the Neutrino Factory

A. Donini^{a,1} and D. Meloni^{b,2}

^a I.N.F.N., Sezione di Roma I and Dip. Fisica, Università di Roma “La Sapienza”,
P.le A. Moro 2, I-00185, Rome, Italy

^b Dip. Fisica, Università di Roma “La Sapienza” and I.N.F.N., Sezione di Roma I,
P.le A. Moro 2, I-00185, Rome, Italy

Abstract

We upgrade the study of the physical reach of a Neutrino Factory in the Four Family Neutrino Mixing scenario taking into account the latest LSND results that points out how the 3+1 scheme cannot be completely ruled out within the present experimental data (although the 2+2 scheme is still the preferred choice when four neutrinos are considered). A detailed comparison of the physical reach of the ν -factory in the two schemes is given, with similar results for the sensitivity to the mixing angles. Huge CP-violating effects can be observed in both schemes with a near, $O(10)$ Km, detector of $O(10)$ Kton size in the $\nu_\mu \rightarrow \nu_\tau$ channel. A smaller detector of 1 Kton size can still observe very large effects in this channel.

¹andrea.donini@roma1.infn.it

²davide.meloni@roma1.infn.it

1 Introduction

Indications in favour of neutrino oscillations have been obtained both in solar neutrino [1, 2, 3, 4, 5] and atmospheric neutrino [6, 7, 8, 9, 10] experiments. The latest atmospheric neutrino data imply $\Delta m_{atm}^2 \sim (1.6 - 4) \times 10^{-3}$ eV² [11], whereas the solar neutrino data prefer $\Delta m_{sun}^2 \sim 10^{-10}$ or $10^{-7} - 10^{-4}$ eV², depending on the particular solution for the solar neutrino deficit. The LSND data [12, 13], on the other hand, would indicate a $\bar{\nu}_\mu \rightarrow \bar{\nu}_e$ oscillation with a third, very distinct, neutrino mass difference: $\Delta m_{LSND}^2 \sim 0.3 - 6$ eV². The LSND evidence in favour of neutrino oscillation has not been confirmed by other experiments so far. However, the MiniBooNE experiment [14] will be able to confirm it or not in the near future. If the LSND results are confirmed we would face three independent evidence for neutrino oscillations characterized by squared mass differences quite well separated. To explain the whole ensemble of data at least four different light neutrino species are needed. The new light neutrino is denoted as sterile [15], since it must be an electroweak singlet to comply with the strong bounds on the Z^0 invisible decay width [16]. We stress that three massive light neutrinos can not explain all the present experimental results, as it has been shown with detailed calculations in [17].

There are two, very different, classes of four neutrino spectra: three almost degenerate neutrinos and an isolated fourth one, or two pairs of almost degenerate neutrinos divided by the large LSND mass gap. The two classes of mass spectra are usually called the 3+1 and 2+2 schemes, respectively. All the present experimental evidence for neutrino oscillations have been combined in the literature in order to identify which of the two classes of mass spectra better adapts to the data. The experimental results were strongly in favour of the 2+2 scheme [18] until the latest LSND results have been presented in June 2000, [19] (see [13]). The new analysis of the experimental data results in a shift of the allowed region towards smaller values of the mixing angle, $\sin^2(2\theta_{LSND})$, reconciling the 3+1 scheme with exclusion bounds coming from CDHS [20], CCFR [21] and Bugey [22]. Although the 2+2 scheme is still favoured³, the 3+1 scheme is at present marginally compatible with the data, [24, 25, 26, 27]. However, the 2+2 and the 3+1 scheme face the upcoming experiments on totally different footing: if MiniBooNE disconfirms LSND, the 2+2 scheme is falsified. On the contrary, it is not possible to falsify the 3+1 scheme: we can always consider an extension of the Standard Model with three light neutrinos and a fourth sterile one, separated by some squared mass difference, $\Delta m_{(1,2,3)-4}^2$. The implication of a negative result of MiniBooNE is just $\Delta m_{(1,2,3)-4}^2 \neq \Delta m_{LSND}^2$.

The specific form of the neutrino mass spectrum appears, therefore, one of the (many) open questions related to the lepton sector of the Standard Model.

Four neutrino oscillations imply a Maki-Nakagawa-Sakata (MNS) 4×4 mixing ma-

³A novel Bayesian analysis of the exclusion bounds, in the spirit of [18] has been presented in [23], claiming that the 3+1 scheme is allowed at the 99 % CL only, but not at the 95 % CL.

trix, with six rotation angles θ_{ij} and three phases δ_i (for Majorana neutrinos, three additional phases are allowed, but they are not testable in oscillation experiments, and therefore will not be considered here). A Neutrino Factory [28, 29] seems to be the best option to explore this huge parameter space. The μ^\pm -decay into the straight section of a muon storage ring should produce a very intense and pure neutrino beam. The rich flavour content (50 % of $\nu_\mu(\bar{\nu}_\mu)$ and 50 % of $\bar{\nu}_e(\nu_e)$ are simultaneously produced), finally, makes the Neutrino Factory well suited for precision studies of the MNS mixing matrix, hopefully including the discovery of leptonic CP-violation [30, 31]. The following scheme reminds that at the Neutrino Factory μ and τ appearance channels can also be used, in combination with the μ and e disappearance experiments.

$$\begin{array}{ccccc}
 & e^-, \tau^- & & & \\
 & \uparrow & & & \\
 & \nu_e, \nu_\tau & & & \\
 & \uparrow & & & \\
 \mu^- \rightarrow e^- & \nu_\mu & \bar{\nu}_e & \rightarrow & \mu^-, e^+ \\
 & \downarrow & & & \\
 & \bar{\nu}_\mu, \bar{\nu}_\tau & & & \\
 & \downarrow & & & \\
 & \mu^+, \tau^+ & & &
 \end{array} \tag{1}$$

In [32, 33, 34] the “wrong-sign muon” channel (μ^+ appearance in a μ^- beam) has been shown to be extremely useful to explore the parameter space of three-family neutrino mixing, with particular interest in the measure of the (single) CP-violating phase, thus deserving the nickname of “golden measurement” at a Neutrino Factory. This has to be compared with a conventional beam experiment (using muon neutrinos from pion decay), such as K2K or the approved FermiLab to Soudan long baseline experiment. In these experiments, mainly the μ -disappearance channel is exploited.

In [35, 36] it was shown that a Neutrino Factory with 10–50 GeV muons can attain $\sin^2(\theta_{ij})$ as low as $10^{-5} - 10^{-3}$ for $\Delta m_{LSND}^2 \in [10^{-1}, 10^1]$ eV². Moreover, it was found that sizeable CP-violating effects can be observed in the $\nu_\mu \rightarrow \nu_\tau$ channel with a 1 Kton detector located at $O(10)$ Km. This analysis has been performed in the 2+2 scheme, the only allowed at that moment. The first motivation for this paper is, therefore, the comparison of what has been found for the 2+2 scheme with the same kind of analysis in the, by now marginally allowed, 3+1 scheme. A better understanding of the oscillation probability structure is a natural by-product of this analysis, both for the CP-conserving and the CP-violating part. In particular, we found a simple argument that shows how the $\nu_\mu \rightarrow \nu_\tau$ channel is the best suited one for CP-violation experiments in four neutrino mixing, to be compared with the three-family mixing where $\nu_e \rightarrow \nu_\mu$ happens to be optimal. Finally, the same argument justifies the loss in sensitivity to small mixing angles in the 3+1 scheme with respect to the 2+2 scheme.

The considered set-up is, as in [35, 36], a Neutrino Factory with $2 \times 10^{20} \mu^+$ and μ^-

decaying in the straight section of a $10 - 50$ GeV muon storage ring per year, and five years of data taking. Muon energies in this range are at present under discussion. The higher energy range allows a good background rejection [37]; moreover, the integrated flux times the cross-section increase with E_μ . A high-energy Neutrino Factory seems therefore the best option, with the energy mainly limited by cost considerations. However, although the total number of charged leptons into the detector increases with the parent muon energy, the flux of low energy neutrinos decreases. If low energy neutrinos are needed (for example, to study CP-violating observables strongly reducing the matter effects [38, 39]), this reduction in the flux should be taken into account.

The mixing angles that relate neutrino mass eigenstates with an LSND mass difference can be studied in short baseline experiments, $L \sim 1$ Km. A small detector with $O(1)$ ton mass is, therefore, well suited to study the whole gap-crossing parameter space (due to the large neutrino flux that illuminates the detector). To take full advantage of the rich flavour content of the beam, this detector should be equipped with τ -tracking and (μ, τ) charge identification. If CP-violating observables are considered, the best option is a larger, $O(10)$ Kton detector located at $O(10)$ Km down the source. This set-up is equally powerful both for the 2+2 and the 3+1 schemes, and should be compared with the typical set-up needed when three-family neutrino mixing is considered.

We also try to answer to the following question: is it possible to explore the whole parameter space with a different detector, with no τ -tracking, but taking full advantage of the energy dependence of the transition probabilities, in the spirit of [32]? We focus on the $\nu_e \rightarrow \nu_\mu$ channel in the 3+1 scheme, with a realistic 10 Kton magnetized iron detector of the type presented in [37] located at $L = 40$ Km down the source. The Neutrino Factory is run with 2×10^{20} useful muons per year for 5 operational years for both muon polarities, at $E_\mu = 50$ GeV, with a detector energy resolution of $\Delta E_\nu = 10$ GeV. A detailed estimate of the backgrounds and detection efficiencies of the considered detector has been presented in [32]. The energy dependence of the oscillation probabilities could in principle help in the measurement of two gap-crossing angles, or one angle and a CP-violating phase, at a time. In the latter case, we find results similar to those in [32]: we can easily reconstruct the phase and the angle at the same time, with an error of tens of degrees on δ_i and of tenths of degree on the angle. However, it seems extremely difficult to measure two gap-crossing angles at a time in the $\nu_e \rightarrow \nu_\mu$ channel. Our conclusion is that to fully explore the parameter space of the four-family model a detector with τ -tracking is needed.

The paper is organized as follows: in Sect. 2 we introduce our parametrization of the MNS mixing matrix both for the 2+2 and 3+1 schemes; in Sect. 2.1 the present bounds on the mixing angles coming from existing experiments are given; in Sect. 2.2 we describe the Neutrino Factory and detector setup; in Sect. 3 we present our results for the sensitivity of the Neutrino Factory to the mixing angles (in the case of no CP violation), comparing the 2+2 and 3+1 schemes; in Sect. 4 we extend our analysis to the CP-violating observables; in Sect. 5 we study the possibility of measuring two gap-

crossing angles or one angle and a phase at a time exploiting the energy dependence of the transition probabilities; in Sect. 6 we eventually draw our conclusions.

2 The Four Neutrino mixing matrix

When four neutrinos are considered, two very different classes of mass spectrum are possible: three almost degenerate (mainly active) neutrinos, accounting for the solar and atmospheric oscillations, separated from the fourth (mainly sterile) one by the large LSND mass difference, Δm_{LSND}^2 ; or, two almost degenerate neutrino pairs, accounting respectively for the solar and atmospheric oscillations, separated by the LSND mass gap. The two mass spectrum classes are depicted in Fig. 1. We refer to these possibilities as 3+1 and 2+2 scenarios. There are four 3+1 and two 2+2 scenarios depending on the specific ordering of the mass differences. Notice that the intriguing hierarchical and inverted hierarchical mass spectrum are 3+1 scenarios.

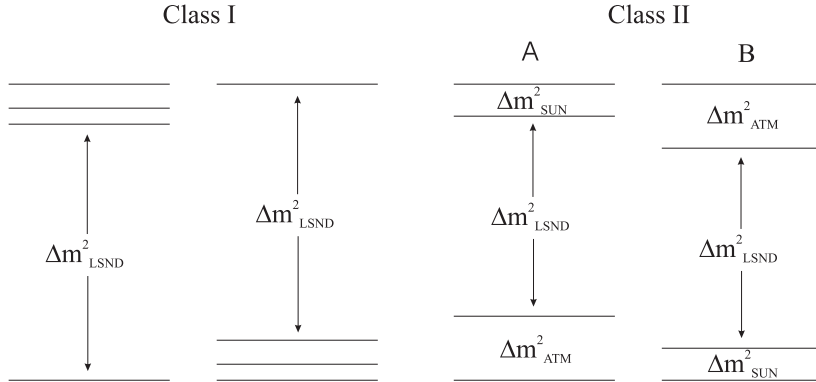


Figure 1: *Different types of four family neutrino mass spectrum: 3+1 scenarios (left); 2+2 scenarios (right).*

It has been shown in [18] that the combined analysis of solar, atmospheric and LSND data disfavours the 3+1 scheme. For this reason, the 2+2 scheme has been carefully studied in the recent literature (see, for example, [40, 41] and references therein). Consider for definiteness the rightmost scenario, namely the lower pair accounting for the solar neutrino deficit and the higher pair for the atmospheric one (the other possibility directly follows by changing the sign of the Δm_{LSND}^2). The ν_μ is therefore in the heavier pair and the ν_e in the lighter one. Is the sterile neutrino, ν_s , responsible for the observed atmospheric oscillations or for the solar neutrino deficit? The latest SuperKamiokande results for the atmospheric neutrinos⁴ disfavours total conversion

⁴ In particular, the zenith angle distribution of the upward-going muons [42], the partially contained multi-ring events and the neutral current data sample.

of ν_μ into the sterile neutrino at 99 % CL [43]. Moreover, the conversion of ν_e solar neutrinos into active neutrinos gives better global fits of the experimental data, with respect to active-into-sterile conversion [44]. Although partial conversion of $\nu_\mu \rightarrow \nu_s$ or $\nu_e \rightarrow \nu_s$ is not excluded (with a sterile component in the atmospheric oscillation as large as 50 %, [45]), the present solar and atmospheric data suggest active-to-active oscillations. The active-to-sterile oscillation should therefore be responsible only for the LSND results. This scenario appears quite unnatural in the framework of the 2+2 scheme.

The latest analysis of the LSND data [19], however, shows a shift of the allowed region for the LSND two-family-equivalent mixing angle, $\sin^2(2\theta_{LSND})$, towards smaller values. This reconciles the 3+1 scheme with the exclusion bounds coming from CDHS [20], CCFR [21] and Bugey [22]. In the 3+1 scheme, the three almost degenerate neutrinos are mainly active and the separated fourth is mainly sterile; the gap-crossing mixing angles are generally small. In this scenario, the interpretation of solar and atmospheric oscillations as active-to-active and LSND as active-to-sterile naturally arises: this scheme is a deformation of the Standard Model, slowly decoupling as the gap-crossing mixing angles become smaller and smaller (and thus, the sterile becomes irrelevant).

Given n light neutrino species, the most general mixing matrix is an $n \times n$ unitary matrix [46], U_{MNS} . For $n = 4$, the MNS matrix contains six independent rotation angles θ_{ij} and three (if neutrinos are Dirac fermions) or six (if neutrinos are Majorana fermions) phases δ_i . However, oscillation experiments are only sensitive to the first three phases, the effect of the Majorana phases being suppressed by factors of m_ν/E_ν . The Majorana or Dirac nature of neutrinos can thus be tested only in $\Delta L = 2$ transitions such as neutrino-less double β -decay [47]. In the following analysis, with no loss in generality, we will restrict ourselves to Dirac-type neutrinos only. We consider a hierarchical 3+1 spectrum and a class II-B 2+2 spectrum, for definiteness.

This large parameter space (6 angles and 3 phases, to be compared with the standard three-family mixing case of 3 angles and 1 phase) is actually reduced to a smaller subspace whenever some of the mass differences become negligible. Consider the measured hierarchy in the mass differences,

$$\Delta m_{sol}^2 \ll \Delta m_{atm}^2 \ll \Delta m_{LSND}^2, \quad (2)$$

and define

$$\Delta_{ij} = \frac{\Delta m_{ij}^2 L}{4E_\nu}. \quad (3)$$

At short distance, $L = O(1)$ Km, for neutrinos up to $O(10)$ GeV,

$$\begin{aligned} \Delta_{sol}, \Delta_{atm} &\ll 1, \\ \Delta_{LSND} &= O(1). \end{aligned} \quad (4)$$

Therefore, it is natural at short distances to neglect the solar and atmospheric mass difference and to work in a reduced parameter space. This approximation is called

“one-mass dominance” [48]. In the 2+2 scheme, neglecting the smaller mass differences implies that rotations in the (1 – 2) and (3 – 4) planes are irrelevant. Thus, it is not possible to measure the rotation angles in these planes in oscillation experiments. Two CP-violating phases also become irrelevant, and therefore the reduced parameter space in the 2+2 scheme contains 4 rotation angles and 1 phase. In the 3+1 scheme, neglecting the solar and atmospheric mass differences implies that rotations in the whole three-dimensional subspace (1 – 2 – 3) are irrelevant for oscillation experiments, and the physical parameter space contains just three rotation angles and no phases. When considering CP-violating phenomena, however, at least two mass differences should be taken into account: in this case we neglect the solar mass difference and consider the atmospheric mass difference a perturbation. This is called “two-mass dominance” approximation. In this approximation, regardless of the scheme, the parameter space contains 5 angles and 2 phases. The number of independent parameters of the MNS mixing matrix in four neutrino models is summarized in Tab. 1.

	Angles	Dirac CP-phases	Majorana CP-phases
Majorana ν 's	6	3	3
Dirac ν 's	6	3	0
Dirac ν 's $\Delta m_{12}^2 = 0$	5	2	0
2+2 Dirac ν 's $\Delta m_{12}^2 = \Delta m_{34}^2 = 0$	4	1	0
3+1 Dirac ν 's $\Delta m_{12}^2 = \Delta m_{34}^2 = 0$	3	0	0

Table 1: *Parameter space in four neutrino models: for Dirac neutrinos we consider the general case (three non-zero mass differences) and the one- and two-mass dominance approximations; for Majorana neutrinos we consider the general case only.*

A generic rotation in a four dimensional space can be obtained by performing six different rotations U_{ij} in the $(i - j)$ plane, resulting in plenty of different parametrizations of the mixing matrix (and still not taking into account the three CP-violating

phases). However, in [35, 36] was shown how the one-mass dominance and two-mass dominance approximations can be implemented in a transparent way (in the sense that only the physical parameters appear in the CP-conserving and CP-violating oscillation probabilities). A convenient parametrization of the mixing matrix is that in which the rotation matrices corresponding to the most degenerate pairs of eigenstates are located at the extreme right. If the eigenstates i and j are degenerate and the matrix U_{ij} is the rightmost one, the corresponding angle θ_{ij} automatically disappears from the oscillation probabilities, and the parameter space gets reduced to the truly observable angles and phases. If a different ordering of the rotation matrices is taken, no angle disappears from the oscillation formulae, and a parameter redefinition would be necessary to reduce the parameter space to the observable sector.

In the 2+2 scheme, the following parametrization was adopted in [35] implementing the previous argument:

$$U_{MNS} = U_{14}(\theta_{14}) U_{13}(\theta_{13}) U_{24}(\theta_{24}) U_{23}(\theta_{23}, \delta_3) U_{34}(\theta_{34}, \delta_2) U_{12}(\theta_{12}, \delta_1). \quad (5)$$

In the one-mass dominance approximation, the unphysical angles and phases (θ_{12}, δ_1) and (θ_{34}, δ_2) automatically decouple. The oscillation probabilities in the appearance channels are⁵:

$$P_{CP}^{2+2}(\nu_e \rightarrow \nu_\mu) = 4c_{13}^2 c_{24}^2 c_{23}^2 s_{23}^2 \sin^2 \left(\frac{\Delta m_{23}^2 L}{4E} \right), \quad (6)$$

$$\begin{aligned} P_{CP}^{2+2}(\nu_e \rightarrow \nu_\tau) = & 4c_{23}^2 c_{24}^2 \left[(s_{13}^2 s_{14}^2 s_{23}^2 + c_{14}^2 c_{23}^2 s_{24}^2) \right. \\ & \left. - 2c_{14} s_{14} c_{23} s_{23} s_{13} s_{24} \cos \delta_3 \right] \sin^2 \left(\frac{\Delta m_{23}^2 L}{4E} \right), \end{aligned} \quad (7)$$

$$\begin{aligned} P_{CP}^{2+2}(\nu_\mu \rightarrow \nu_\tau) = & 4c_{23}^2 c_{13}^2 \left[(s_{13}^2 s_{14}^2 c_{23}^2 + c_{14}^2 s_{23}^2 s_{24}^2) \right. \\ & \left. + 2c_{14} s_{14} c_{23} s_{23} s_{13} s_{24} \cos \delta_3 \right] \sin^2 \left(\frac{\Delta m_{23}^2 L}{4E} \right); \end{aligned} \quad (8)$$

in the disappearance channels are:

$$P_{CP}^{2+2}(\nu_\mu \rightarrow \nu_\mu) = 1 - 4c_{13}^2 c_{23}^2 (s_{23}^2 + s_{13}^2 c_{23}^2) \sin^2 \left(\frac{\Delta m_{23}^2 L}{4E} \right), \quad (9)$$

$$P_{CP}^{2+2}(\nu_e \rightarrow \nu_e) = 1 - 4c_{23}^2 c_{24}^2 (s_{24}^2 + s_{23}^2 c_{24}^2) \sin^2 \left(\frac{\Delta m_{23}^2 L}{4E} \right). \quad (10)$$

Notice that the physical phase δ_3 appears in the CP-conserving transition probabilities in a pure cosine dependence. No CP-odd observable can be built out of the oscillation probabilities in this approximation in spite of the existence of a physical phase in the mixing matrix.

⁵ In what follows, we separate the CP-even terms from the CP-odd ones:

$P(\nu_\alpha \rightarrow \nu_\beta) = P_{CP}(\nu_\alpha \rightarrow \nu_\beta) + P_{CP}(\nu_\alpha \rightarrow \nu_\beta)$.

In the two-mass dominance approximation, new CP-violating terms arise. Expanding the probabilities at first order in Δ_{atm} , we get⁶:

$$\begin{aligned} P_{CP}^{2+2}(\nu_e \rightarrow \nu_\mu) &= -8c_{13}^2 c_{23}^2 c_{24} c_{34} s_{23} s_{24} s_{34} \sin(\delta_2 + \delta_3) \\ &\times \left(\frac{\Delta m_{34}^2 L}{4E_\nu} \right) \sin^2 \left(\frac{\Delta m_{23}^2 L}{4E_\nu} \right), \end{aligned} \quad (11)$$

$$\begin{aligned} P_{CP}^{2+2}(\nu_e \rightarrow \nu_\tau) &= 8c_{23} c_{24} \left\{ c_{23} c_{34} s_{23} s_{24} s_{34} (c_{14}^2 - s_{13}^2 s_{14}^2) \sin(\delta_2 + \delta_3) \right. \\ &+ c_{14} c_{34} s_{13} s_{14} s_{34} \left[(s_{24}^2 - s_{23}^2) \sin \delta_2 - s_{23}^2 s_{24}^2 \sin(\delta_2 + 2\delta_3) \right] \\ &+ c_{14} c_{24} s_{13} s_{14} s_{23} s_{24} (c_{34}^2 - s_{34}^2) \sin \delta_3 \left. \right\} \\ &\times \left(\frac{\Delta m_{34}^2 L}{4E_\nu} \right) \sin^2 \left(\frac{\Delta m_{23}^2 L}{4E_\nu} \right), \end{aligned} \quad (12)$$

$$\begin{aligned} P_{CP}^{2+2}(\nu_\mu \rightarrow \nu_\tau) &= -8c_{13}^2 c_{23}^2 c_{14} c_{24} c_{34} s_{34} [c_{23} s_{13} s_{14} \sin \delta_2 + c_{14} s_{23} s_{24} \sin(\delta_2 + \delta_3)] \\ &\times \left(\frac{\Delta m_{34}^2 L}{4E} \right) \sin^2 \left(\frac{\Delta m_{23}^2 L}{4E} \right). \end{aligned} \quad (13)$$

Two distinct phases, δ_2 and δ_3 , appear in these formulae in a characteristic sine dependence which is the trademark of CP-violating observables. CP-violating effects can only be measured in appearance channels, whereas the disappearance channels $\nu_e \rightarrow \nu_e$ and $\nu_\mu \rightarrow \nu_\mu$ are only sensitive to the CP-even parameters,

$$P_{CP}(\nu_e \rightarrow \nu_e) = P_{CP}(\nu_\mu \rightarrow \nu_\mu) = P_{CP}(\nu_\tau \rightarrow \nu_\tau) = 0. \quad (14)$$

In the 3+1 scheme, the following parametrization shares the same virtues of eq. (5):

$$U_{MNS} = U_{14}(\theta_{14}) U_{24}(\theta_{24}) U_{34}(\theta_{34}) U_{23}(\theta_{23}, \delta_3) U_{13}(\theta_{13}, \delta_2) U_{12}(\theta_{12}, \delta_1). \quad (15)$$

This parametrization has the additional advantage that the three-family model mixing matrix in its standard form can be immediately recovered when $\theta_{i4} = 0$. For small gap-crossing angles θ_{i4} , we expect slight modification with respect to the three-family model.

In the one-mass dominance approximation, the unphysical angles and phases (θ_{12}, δ_1) , (θ_{13}, δ_2) and (θ_{23}, δ_3) automatically decouple. The oscillation probabilities in the appearance channels are:

$$P_{CP}^{3+1}(\nu_e \rightarrow \nu_\mu) = 4c_{24}^2 c_{34}^4 s_{14}^2 s_{24}^2 \sin^2 \left(\frac{\Delta m_{34}^2 L}{4E} \right), \quad (16)$$

$$P_{CP}^{3+1}(\nu_e \rightarrow \nu_\tau) = 4c_{24}^2 c_{34}^2 s_{14}^2 s_{34}^2 \sin^2 \left(\frac{\Delta m_{34}^2 L}{4E} \right), \quad (17)$$

$$P_{CP}^{3+1}(\nu_\mu \rightarrow \nu_\tau) = 4c_{34}^2 s_{24}^2 s_{34}^2 \sin^2 \left(\frac{\Delta m_{34}^2 L}{4E} \right); \quad (18)$$

⁶In [35, 36] some misprints were present in the $\nu_e \rightarrow \nu_\tau$ formula that have been corrected here.

in the disappearance channels are:

$$P_{CP}^{3+1}(\nu_\mu \rightarrow \nu_\mu) = 1 - 4c_{34}^2 s_{24}^2 (c_{24}^2 + s_{24}^2 s_{34}^2) \sin^2 \left(\frac{\Delta m_{34}^2 L}{4E} \right), \quad (19)$$

$$P_{CP}^{3+1}(\nu_e \rightarrow \nu_e) = 1 - 4c_{24}^2 c_{34}^2 s_{14}^2 (1 - s_{14}^2 c_{24}^2 c_{34}^2) \sin^2 \left(\frac{\Delta m_{34}^2 L}{4E} \right). \quad (20)$$

As already stressed, angles and phases in the three-dimensional physically irrelevant subspace are not present in these formulae.

Finally, in the two-mass dominance approximation we get, expanding at first order in Δ_{atm} :

$$\begin{aligned} P_{CP}^{3+1}(\nu_e \rightarrow \nu_\mu) &= 8 c_{34}^2 c_{23} c_{24} s_{14} s_{24} \{ -c_{13} s_{14} s_{23} s_{34} \sin \delta_2 \\ &+ c_{14} s_{13} [c_{13} c_{23} s_{24} s_{34} \sin \delta_3 + c_{24} s_{23} \sin(\delta_2 - \delta_3)] \} \\ &\times \left(\frac{\Delta m_{23}^2 L}{4E_\nu} \right) \sin^2 \left(\frac{\Delta m_{34}^2 L}{4E_\nu} \right), \end{aligned} \quad (21)$$

$$\begin{aligned} P_{CP}^{3+1}(\nu_e \rightarrow \nu_\tau) &= 8 c_{34}^2 c_{13} c_{23} c_{24} s_{14} s_{34} [s_{14} s_{23} s_{24} \sin \delta_2 - c_{14} c_{23} s_{13} \sin \delta_3] \\ &\times \left(\frac{\Delta m_{23}^2 L}{4E_\nu} \right) \sin^2 \left(\frac{\Delta m_{34}^2 L}{4E_\nu} \right), \end{aligned} \quad (22)$$

$$\begin{aligned} P_{CP}^{3+1}(\nu_\mu \rightarrow \nu_\tau) &= -8 c_{34}^2 c_{23} c_{24} s_{23} s_{24} s_{34} \sin \delta_2 \\ &\times \left(\frac{\Delta m_{23}^2 L}{4E} \right) \sin^2 \left(\frac{\Delta m_{34}^2 L}{4E} \right). \end{aligned} \quad (23)$$

These formulae, both in the 2+2 and the 3+1 scheme, will be used in Sect. 3 and Sect. 4 to explore the parameter space of the four-family model at the Neutrino Factory.

2.1 Experimental bounds on the gap-crossing angles

We recall here the bounds on the rotation angles and mass differences coming from the existing experiments. The Bugey and CHOOZ experiments [22, 49] give strong upper limit to the $\nu_e \rightarrow \nu_e$ disappearance two-family equivalent mixing angle. In two families,

$$P_{CP}(\nu_e \rightarrow \nu_e) = 1 - \sin^2(2\theta)_{exp} \sin^2 \left(\frac{\Delta m_{LSND}^2 L}{4E} \right) \quad (24)$$

with $\sin^2(2\theta)_{exp} \leq 0.2$ in the LSND-allowed region. The positive result from LSND gives a lower limit on the $\nu_e \rightarrow \nu_\mu$ two-family-equivalent mixing angle,

$$P_{CP}(\nu_\mu \rightarrow \nu_e) = \sin^2(2\theta)_{LSND} \sin^2 \left(\frac{\Delta m_{LSND}^2 L}{4E} \right) \quad (25)$$

with $10^{-3} \leq \sin^2(2\theta)_{LSND} \leq 1$. These bounds, jointly with the negative results from Karmen2 [50] and previous experiments such as CDHS and CCFR [20, 21], must be interpreted in the 2+2 and 3+1 scheme, extracting informations on the gap-crossing angles and mass differences.

- **The 2+2 scheme**

In the 2+2 scheme, that is still favoured by the data, the bound on ν_e disappearance translates into an upper limit on the combination

$$c_{23}^2 \sin^2(2\theta_{24}) + c_{24}^4 \sin^2(2\theta_{23}) \leq 0.2 , \quad (26)$$

whereas the bound on ν_e appearance implies

$$10^{-3} \leq c_{13}^2 c_{24}^2 \sin^2(2\theta_{23}) \leq 10^{-2} . \quad (27)$$

These bounds suggest the conservative (or even “pessimistic”) hypothesis adopted in [35]: to consider the four gap-crossing angles $\theta_{13}, \theta_{14}, \theta_{23}$ and θ_{24} to be equally small in the mass difference region $\Delta m_{LSND}^2 \in [10^{-1}, 10^1] \text{ eV}^2$. We follow here the same hypothesis: all the gap-crossing angles are small (i.e. less than 10°), with the possible exception of one angle that we leave to vary in some interval. The remaining angles θ_{12} and θ_{34} are directly the solar and atmospheric mixing angles in the two-family parametrization, respectively. The typical flavour content of the mass eigenstates in the 2+2 scheme is presented in Fig. 2 (left).

- **The 3+1 scheme**

This scheme is only marginally allowed (a recent study [23] shows that it is compatible with the experimental data at the 99 % CL only). However, it is a natural extension of the three-family model. There are four very small allowed region in the two-family equivalent parameter space [24]:

1. $\Delta m_{34}^2 \simeq 0.3 \text{ eV}^2$; $\sin^2(2\theta)_{LSND} \simeq 2 \times 10^{-2}$;
2. $\Delta m_{34}^2 \simeq 0.9 \text{ eV}^2$; $\sin^2(2\theta)_{LSND} \simeq 2 \times 10^{-3}$;
3. $\Delta m_{34}^2 \simeq 1.7 \text{ eV}^2$; $\sin^2(2\theta)_{LSND} \simeq 1 \times 10^{-3}$;
4. $\Delta m_{34}^2 \simeq 6.0 \text{ eV}^2$; $\sin^2(2\theta)_{LSND} \simeq 2 \times 10^{-3}$.

We restrict ourselves to case 2, for simplicity. In this case, we get in our parametrization for the ν_e appearance mixing parameter

$$c_{34}^4 s_{14}^2 \sin^2(2\theta_{24}) \simeq 2 \times 10^{-3} . \quad (28)$$

This bound is consistent with the conservative hypothesis of equally small gap-crossing angles θ_{i4} , that will be followed in the rest of the paper. In the 3+1 scheme the remaining angles, θ_{12}, θ_{23} and θ_{13} can be obtained by the combined analysis of solar and atmospheric data in the three-family parametrization. The typical flavour content of the mass eigenstates in the 3+1 scheme is presented in Fig. 2 (right).



Figure 2: *The flavour content in the mass eigenstates with a representative choice for the mixing angles: in the 2+2 scheme with $\theta_{12} = 45^\circ, \theta_{34} = 45^\circ, \theta_{13} = \theta_{14} = \theta_{23} = \theta_{24} = 5^\circ$ (left); in the 3+1 scheme with $\theta_{12} = 45^\circ, \theta_{13} = 13^\circ, \theta_{23} = 45^\circ, \theta_{14} = \theta_{24} = \theta_{34} = 5^\circ$ (right). The different flavours are, from lightest to darkest: ν_s ; ν_μ ; ν_e and ν_τ .*

2.2 Experimental Setup: The Neutrino Factory and the Detector

In the muon rest frame, the distribution of muon antineutrinos (neutrinos) and electron neutrinos (antineutrinos) in the decay $\mu^\pm \rightarrow e^\pm + \nu_e (\bar{\nu}_e) + \bar{\nu}_\mu (\nu_\mu)$ is given by:

$$\frac{d^2N}{dxd\Omega} = \frac{1}{4\pi} [f_0(x) \mp \mathcal{P}_\mu f_1(x) \cos \vartheta], \quad (29)$$

where E_ν denotes the neutrino energy, $x = 2E_\nu/m_\mu$ and \mathcal{P}_μ is the average muon polarization along the beam directions. ϑ is the angle between the neutrino momentum vector and the muon spin direction and m_μ is the muon mass. The positron (electron) neutrino flux is identical in form to that for muon neutrinos (antineutrinos), when the electron mass is neglected. The functions f_0 and f_1 are given in Table 2, [51]. In the laboratory frame, the neutrino fluxes, boosted along the muon momentum vector, are given by:

$$\begin{aligned} \frac{d^2N_{\bar{\nu}_\mu, \nu_\mu}}{dyd\Omega} &= \frac{4n_\mu}{\pi L^2 m_\mu^6} E_\mu^4 y^2 (1 - \beta \cos \varphi) \left\{ \left[3m_\mu^2 - 4E_\mu^2 y (1 - \beta \cos \varphi) \right] \right. \\ &\quad \left. \mp \mathcal{P}_\mu \left[m_\mu^2 - 4E_\mu^2 y (1 - \beta \cos \varphi) \right] \right\}, \\ \frac{d^2N_{\nu_e, \bar{\nu}_e}}{dyd\Omega} &= \frac{24n_\mu}{\pi L^2 m_\mu^6} E_\mu^4 y^2 (1 - \beta \cos \varphi) \left\{ \left[m_\mu^2 - 2E_\mu^2 y (1 - \beta \cos \varphi) \right] \right. \\ &\quad \left. \mp \mathcal{P}_\mu \left[m_\mu^2 - 2E_\mu^2 y (1 - \beta \cos \varphi) \right] \right\}. \end{aligned} \quad (30)$$

	$f_0(x)$	$f_1(x)$
ν_μ, e	$2x^2(3 - 2x)$	$2x^2(1 - 2x)$
ν_e	$12x^2(1 - x)$	$12x^2(1 - x)$

Table 2: *Flux functions.*

Here, $\beta = \sqrt{1 - m_\mu^2/E_\mu^2}$, E_μ is the parent muon energy, $y = E_\nu/E_\mu$, n_μ is the number of useful muons per year obtained from the storage ring and L is the distance to the detector. φ is the angle between the beam axis and the direction pointing towards the detector. We shall consider in what follows as a “reference set-up” a neutrino beam resulting from the decay of $n_\mu = 2 \times 10^{20}$ unpolarized positive and/or negative muons in one of the straight sections of a muon storage ring (i.e. we do not consider two baselines operating at the same time) per year. The collected muons have energy E_μ in the range $10 - 50$ GeV. This energy range is under discussion as a convenient goal (a definite answer on which is the optimal energy to run the Neutrino Factory is still missing). The angular divergence $\delta\varphi$ is taken to be constant, $\delta\varphi \sim 0.1$ mr.

The charged current neutrino and antineutrino interaction rates can be computed using the approximate expressions for the neutrino-nucleon cross sections on an isoscalar target⁷,

$$\sigma_{\nu N} \sim 0.67 \times 10^{-42} \times \frac{E_\nu}{GeV} \times m^2 \quad \sigma_{\bar{\nu} N} \sim 0.34 \times 10^{-42} \times \frac{E_\nu}{GeV} \times m^2 . \quad (31)$$

To explore the whole CP-conserving parameter space we need a detector with τ tracking and (μ, τ) charge identification capability. As the dominant signals are expected to peak at $L/E_\nu \sim 1/\Delta m_{LSND}^2$, most of the parameter space can be explored in short baseline experiments (SLB), with $L \sim 1$ Km. At such a short distance from the source the neutrino flux is so intense that a small detector is well suited to study CP-conserving transitions. In what follows we consider an hypothetical 1 ton detector, with no detailed calculation of background and efficiencies as a function of the neutrino energy. We consider a constant background B at the level of 10^{-5} of the expected number of charged current events, N_{CC} , and a constant reconstruction efficiency $\epsilon_\mu = 0.5$ for μ^\pm and $\epsilon_\tau = 0.35$ for τ^\pm . The number of expected charged leptons in absence of oscillation is $N_{\mu^-} = 9.3 \times 10^8$ and $N_{e^+} = 4.0 \times 10^8$ for a μ^- beam ($N_{\mu^+} = 4.7 \times 10^8$ and $N_{e^-} = 7.9 \times 10^8$ for a μ^+ beam). We also applied a conservative cut on the neutrino energy: neutrinos with $E_\nu \leq 5$ GeV have not been included in our results.

To extend our analysis to the CP-violating parameter space, a larger detector must be considered: we choose an hypothetical 10 Kton detector, located a bit farther from the neutrino source, at $L = O(10 - 100)$ Km. Also in this case μ and τ charge identification capability is needed, being the $\nu_\mu \rightarrow \nu_\tau$ transitions the optimal channel to observe CP-violation in a four-family model (as will be explained in the following). The same background and reconstruction efficiencies as for the CP-conserving sector are included, and again a fiducial cut on neutrinos with $E_\nu \leq 5$ GeV is applied.

⁷For the ν_τ -nucleon interaction, we used the exact expression for the cross section taking into account the τ -mass.

3 Sensitivity reach of the Neutrino Factory

We concentrate now on the sensitivity to the different gap-crossing angles that appear in the oscillation probabilities when only the LSND mass difference is taken into account, namely eqs. (6-10) for the 2+2 scheme and eqs. (16-20) for the 3+1 scheme⁸.

We define the sensitivity in the appearance channel as follows: the number of total expected events for a given flavour ν_α is

$$N_{tot} = N_\alpha^B \pm \Delta N_\alpha^B + N_\beta \quad (32)$$

where

$$N_\alpha^B = N_\alpha \cdot B, \quad (33)$$

$$N_\beta = N_\alpha < P(\nu_\alpha \rightarrow \nu_\beta) >, \quad (34)$$

with N_α the number of expected events in the absence of oscillation, B the fractional background (we consider $B = 10^{-5}$) and $< P(\nu_\alpha \rightarrow \nu_\beta) >$ the transition probability averaged over the ν_α flux and the CC interaction cross-section. Fluctuations over the background are taken to be gaussian, $\Delta N_\alpha^B = \sqrt{N_\alpha^B}$. The excluded zone at 90 % CL (following [52]) if no event is observed is the region to the right of

$$N_\beta = 1.65 \Delta N_\alpha^B. \quad (35)$$

The sensitivity in the disappearance channel is defined as follows: the number of total expected events for a given flavour ν_α is

$$N_{tot} = N_\alpha \cdot (1 - B) \pm \Delta[N_\alpha \cdot (1 - B)] - N_\beta \quad (36)$$

where

$$N_\beta = \sum_{\beta \neq \alpha} N_\alpha < P(\nu_\alpha \rightarrow \nu_\beta) > \quad (37)$$

summing over all flavours distinct from ν_α . In this case we compare N_β with the gaussian fluctuation over $N_\alpha \times (1 - B)$ (we notice that a background B at the level of 10^{-5} plays a marginal role, with respect to the appearance case). Again, following [52], if no event is observed the region to the right of

$$N_\beta = 1.65 \Delta[N_\alpha \cdot (1 - B)] \quad (38)$$

is excluded at 90 % CL.

⁸ Although we refer to the one- or two-mass dominance approximation (in the section devoted to CP-violating observables) formulae, all the numerical results have been obtained with the exact expressions for the transition probabilities.

3.1 Sensitivity in the 2+2 scheme

We recall here the results of [35, 36, 53], albeit rederived with slightly different input parameters. In the one-mass dominance approximation, the CP-conserving parameter space consists of four rotation angles ($\theta_{13}, \theta_{14}, \theta_{23}$ and θ_{24}) and one phase, δ_3 . In what follows we set $\delta_3 = 0$. The useful channels to measure or put severe upper limits on the gap-crossing angles at the Neutrino Factory are the following (for a μ^- decay):

$$\begin{aligned}
 \bar{\nu}_e &\rightarrow \bar{\nu}_\mu \rightarrow \mu^+ & (\mu^+ \text{ appearance}) \\
 \nu_\mu &\rightarrow \nu_\mu \rightarrow \mu^- & (\mu^- \text{ disappearance}) \\
 \bar{\nu}_e &\rightarrow \bar{\nu}_\tau \rightarrow \tau^+ & (\tau^+ \text{ appearance}) \\
 \nu_\mu &\rightarrow \nu_\tau \rightarrow \tau^- & (\tau^- \text{ appearance}). \tag{39}
 \end{aligned}$$

In order to present the sensitivity to a specific $\sin^2 \theta$, we adopt the following approach: we vary $\sin^2 \theta$ between 10^{-7} and 1; the remaining three angles are considered to be already known: two of them are fixed to a small value, $\theta_{ij} = 2^\circ$, and the third one is varied from 1° to 60° . The remaining parameters (those measured in solar and atmospheric experiments) are taken as follows:

$$\begin{aligned}
 \theta_{12} &= 45^\circ, \theta_{34} = 45^\circ; \\
 \Delta m_{12}^2 &= 10^{-4} \text{eV}^2, \Delta m_{34}^2 = 3.5 \times 10^{-3} \text{eV}^2.
 \end{aligned}$$

The large mass difference Δm_{23}^2 is varied from 10^{-3} to 10^2 eV 2 . At $L = 1$ Km matter effects are not relevant, since such a baseline is short enough to be completely above ground. We consider 2×10^{20} useful muons per year and 5 years of data taking, with $E_\mu = 20$ GeV. For simplicity, the Neutrino Factory is supposed to be working with negative muons only.

- **Sensitivity to $\sin^2 \theta_{23}$: μ^+ appearance**

The μ^+ appearance channel (the so-called “wrong-sign” muons) is particularly sensitive to θ_{23} . Fig. 3 shows the 90 % CL exclusion curve in the $\sin^2 \theta_{23}/\Delta m_{23}^2$ plane for different values of θ_{13} . In the LSND-allowed region (Δm_{23}^2 in the $10^{-1} - 10^1$ eV 2 range) the dependence on θ_{13} is mild: $\sin^2 \theta_{23}$ can reach 10^{-6} for $\theta_{13} \simeq 1^\circ$ or 6×10^{-6} for $\theta_{13} \simeq 60^\circ$.

- **Sensitivity to $\sin^2 \theta_{13}$: μ^- disappearance**

In Fig. 4 we present the 90 % CL exclusion curve in the $\sin^2 \theta_{13}/\Delta m_{23}^2$ plane, at different values of $\theta_{23} = 1^\circ, 10^\circ$ and 30° , for the μ^- disappearance channel. In [35] it was observed that this channel proves more sensitive to $\sin^2 \theta_{13}$ than the μ^+ appearance one for small values of θ_{23} . On the contrary, the μ^+ appearance channel has the larger

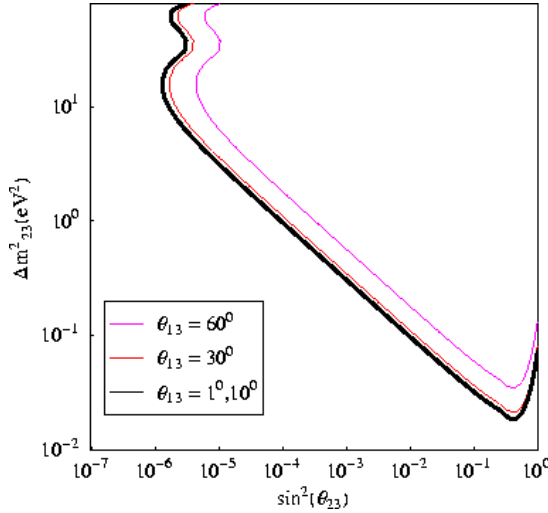


Figure 3: *Sensitivity reach in the $\sin^2 \theta_{23}/\Delta m_{23}^2$ plane at different values of $\theta_{13} = 1^\circ, 10^\circ, 30^\circ$ and 60° for μ^+ appearance in the 2+2 scheme.*

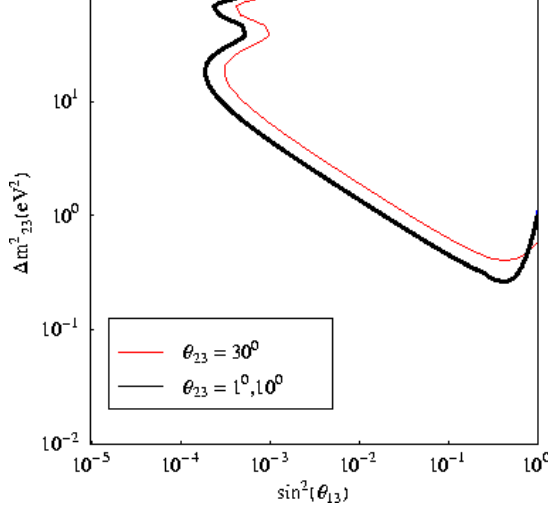


Figure 4: *Sensitivity reach in the $\sin^2 \theta_{13}/\Delta m_{23}^2$ plane at different values of $\theta_{23} = 1^\circ, 10^\circ$ and 30° for μ^- disappearance in the 2+2 scheme.*

sensitivity attained for large values of θ_{23} , a scenario somewhat disfavoured by the LSND measurement. In the μ^- disappearance channel, the Neutrino Factory can put an upper bound to $\sin^2 \theta_{13}$ at the $10^{-4} - 10^{-2}$ level for Δm_{23}^2 in the $10^{-1} - 10^1$ eV² range.

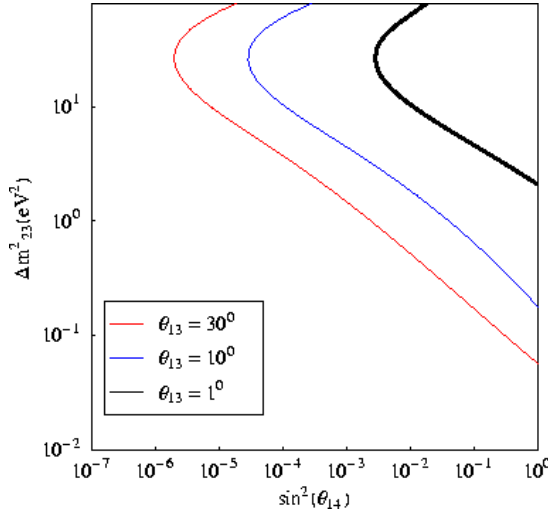


Figure 5: *Sensitivity reach in the $\sin^2 \theta_{14}/\Delta m_{23}^2$ plane at different values of $\theta_{13} = 1^\circ, 10^\circ$ and 30° for τ^- appearance in the 2+2 scheme.*

- **Sensitivity to $\sin^2 \theta_{14}$ and $\sin^2 \theta_{24}$: τ^- appearance**

The τ^- appearance channel is quite sensitive to both $\sin^2 \theta_{14}$ and $\sin^2 \theta_{24}$. Fig. 5 illustrates the sensitivity to $\sin^2 \theta_{14}$ as a function of θ_{13} : for about 1° , sensitivities of the order of 10^{-2} are attainable, while for 10° values as small as 4×10^{-5} can be reached. For even larger values of θ_{13} it goes down to 10^{-6} (we recall that θ_{13} is not severely constrained by the Bugey-CHOOZ experimental bounds, eq. (26)).

Fig. 6 depicts the foreseeable sensitivity reach to $\sin^2 \theta_{24}$ as a function of θ_{23} : for small values of θ_{23} the sensitivity to $\sin^2 \theta_{24}$ attains level as low as 10^{-6} .

In contrast, the τ^+ appearance channel looks less promising, for $\delta_3 = 0$. Due to the relative negative sign between the two terms in the analytic expression for $P(\nu_e \rightarrow \nu_\tau)$, eq. (7), cancellations for particular values of the angles occur, resulting in a decreasing sensitivity in specific regions of the parameter space. This sensitivity suppression is absent in the τ^- channel as the relative sign between the two terms in $P(\nu_\mu \rightarrow \nu_\tau)$, eq. (8), is positive⁹.

3.2 Sensitivity in the 3+1 scheme

In the one-mass dominance approximation, the CP-conserving parameter space consists of three rotation angles (θ_{14}, θ_{24} and θ_{34}) and no phases. The useful channels to measure

⁹ The same argument holds, albeit interchanging the two channels, for $\delta_3 = \pi$.

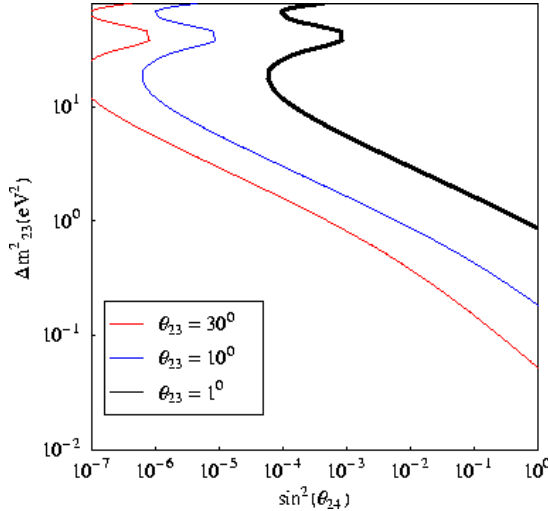


Figure 6: *Sensitivity reach in the $\sin^2 \theta_{24}/\Delta m_{23}^2$ plane at different values of $\theta_{23} = 1^\circ, 10^\circ$ and 30° for τ^- appearance in the 2+2 scheme.*

or put severe upper limits on the gap-crossing angles at the Neutrino Factory are (for a μ^- decay):

$$\begin{aligned} \bar{\nu}_e &\rightarrow \bar{\nu}_\mu \rightarrow \mu^+ & (\mu^+ \text{ appearance}) \\ \nu_\mu &\rightarrow \nu_\tau \rightarrow \tau^- & (\tau^- \text{ appearance}). \end{aligned} \quad (40)$$

We will see in the following that these two channels are optimal to study the whole CP-conserving 3+1 parameter space.

We adopt the same approach as for the 2+2 scheme: we vary $\sin^2 \theta$ between 10^{-7} and 1; the other two angles are considered to be already known: one of them is fixed to a small value, $\theta_{ij} = 2^\circ$, and the second one is varied from 1° to 60° . The remaining parameters (those measured in solar and atmospheric experiments) are taken, following [54], as:

$$\begin{aligned} \theta_{12} &= 22.5^\circ, \theta_{13} = 13^\circ, \theta_{23} = 45^\circ; \\ \Delta m_{12}^2 &= 10^{-4} \text{eV}^2, \Delta m_{23}^2 = 3.5 \times 10^{-3} \text{eV}^2. \end{aligned}$$

We consider 2×10^{20} useful muons per year and 5 years of data taking, with $E_\mu = 20$ GeV.

- **Sensitivity to $\sin^2 \theta_{14}$ and $\sin^2 \theta_{24}$: μ^+ appearance**

The μ^+ appearance channel is particularly sensitive to both $\sin^2 \theta_{14}$ and $\sin^2 \theta_{24}$. Fig. 7 shows the 90 % CL exclusion curve in the $\sin^2 \theta_{14}/\Delta m_{34}^2$ plane (left) and in the

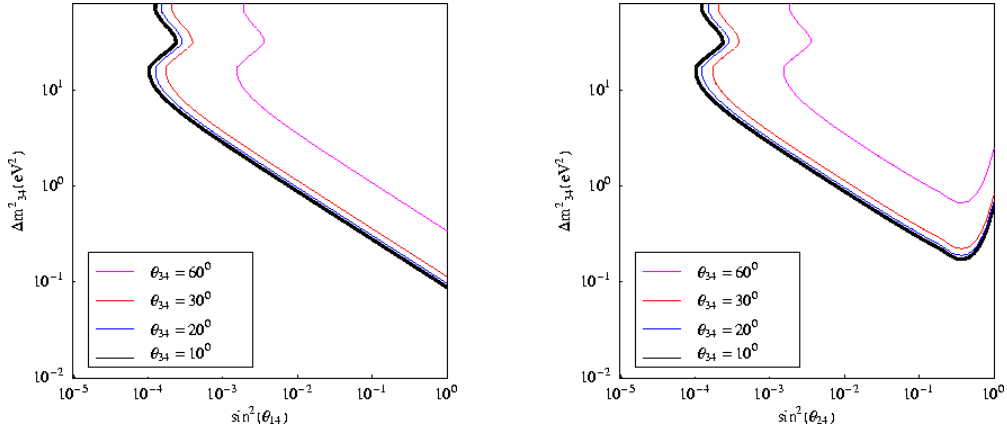


Figure 7: *Sensitivity reach in the $\sin^2 \theta_{14}/\Delta m_{34}^2$ plane (left) and in the $\sin^2 \theta_{24}/\Delta m_{34}^2$ plane (right) at different values of $\theta_{34} = 1^\circ, 10^\circ, 30^\circ$ and 60° for μ^+ appearance in the 3+1 scheme.*

$\sin^2 \theta_{24}/\Delta m_{34}^2$ plane (right) for different values of θ_{34} . The dependence on θ_{34} is very mild for small values of θ_{34} . In the LSND-allowed region, $\Delta m_{34}^2 \in [10^{-1}, 10^1] \text{ eV}^2$, both $\sin^2 \theta_{14}$ and $\sin^2 \theta_{24}$ can reach 10^{-4} for $\theta_{34} \leq 30^\circ$ or 10^{-3} for $\theta_{34} \simeq 60^\circ$.

The μ^- disappearance channel is not sensitive to θ_{14} , but can explore approximately the same region as the appearance channel in the $\sin^2 \theta_{24}/\Delta m_{34}^2$ plane, see Fig. 8.

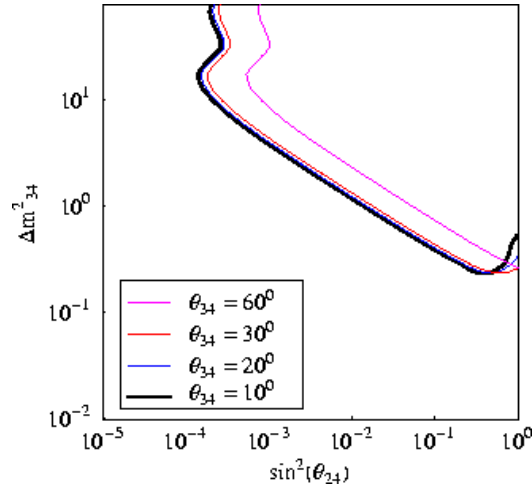


Figure 8: *Sensitivity reach in the $\sin^2 \theta_{24}/\Delta m_{34}^2$ plane at different values of $\theta_{34} = 1^\circ, 10^\circ, 30^\circ$ and 60° for μ^- disappearance in the 3+1 scheme.*

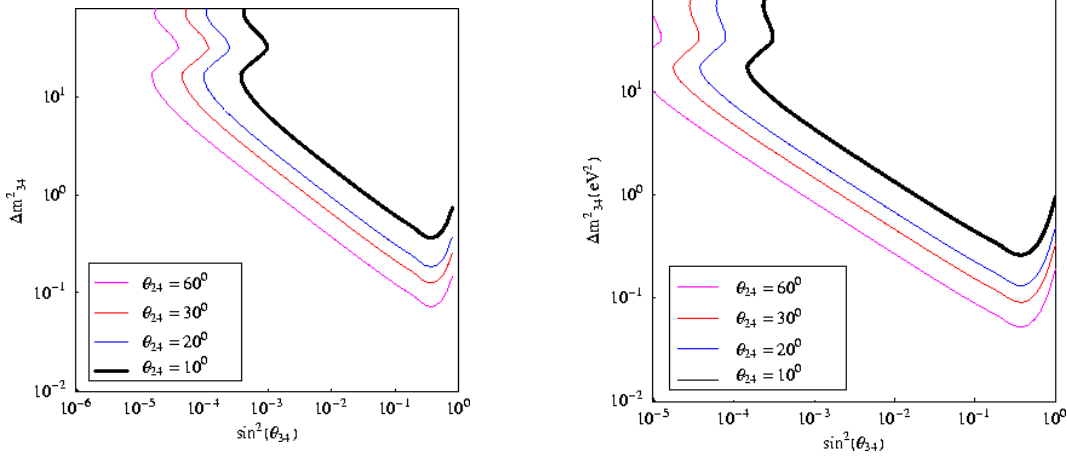


Figure 9: *Sensitivity reach in the $\sin^2 \theta_{34}/\Delta m_{34}^2$ plane at different values of $\theta_{14} = 1^\circ, 10^\circ, 30^\circ$ and 60° for τ^+ appearance in the 3+1 scheme (left) and at different values of $\theta_{24} = 1^\circ, 10^\circ, 30^\circ$ and 60° for τ^- appearance in the 3+1 scheme (right).*

- **Sensitivity to $\sin^2 \theta_{34}$: τ appearance**

Both τ appearance channel are equally sensitive to $\sin^2 \theta_{34}$, as can be seen in eqs. (17) and (18). Fig. 9 shows the 90 % CL exclusion curve in the $\sin^2 \theta_{34}/\Delta m_{34}^2$ plane for τ^+ appearance at different values of θ_{14} (left) and for τ^- appearance at different values of θ_{24} (right). In the LSND-allowed region, $\sin^2 \theta_{34}$ can reach some units in 10^{-5} for $\theta_{14}, \theta_{24} \leq 30^\circ$ or 10^{-5} for $\theta_{14}, \theta_{24} \simeq 60^\circ$.

3.3 Remarks and conclusions on the sensitivity reach

The results of the previous subsections show that a Neutrino Factory with $n_\mu = 2 \times 10^{20}$ useful muons per year and a small detector of $O(1)$ ton size with τ tracking and (μ, τ) charge identification capability can severely constrain the whole four-family model CP-conserving parameter space, both in the 2+2 scheme and 3+1 scheme. In the former, the sensitivity reach to all gap-crossing angles in the LSND-allowed region is at the level of $\sin^2 \theta \geq 10^{-6} - 10^{-4}$, depending on the specific angle considered. In the latter the sensitivity reach is at the level of $\sin^2 \theta \geq 10^{-5} - 10^{-3}$, depending on the specific angle considered, slightly less than in the 2+2 case.

This results can be easily understood in terms of a simple power counting argument. Consider the gap-crossing angles equally small, $\sin \theta_{ij} \simeq \epsilon$ (with θ_{ij} some gap-crossing angle in the 2+2 or the 3+1 scheme). In the 2+2 scheme, the CP-conserving transition

probabilities become:

$$\begin{aligned}
P_{CP}^{2+2}(\nu_e \rightarrow \nu_\mu) &= 4\epsilon^2 \sin^2 \left(\frac{\Delta m_{23}^2 L}{4E} \right) + O(\epsilon^4) , \\
P_{CP}^{2+2}(\nu_e \rightarrow \nu_\tau) &= 4\epsilon^2 \sin^2 \left(\frac{\Delta m_{23}^2 L}{4E} \right) + O(\epsilon^4) , \\
P_{CP}^{2+2}(\nu_\mu \rightarrow \nu_\tau) &= O(\epsilon^4) , \\
P_{CP}^{2+2}(\nu_\mu \rightarrow \nu_\mu) &= P_{CP}^{2+2}(\nu_e \rightarrow \nu_e) = 1 - 8\epsilon^2 \sin^2 \left(\frac{\Delta m_{23}^2 L}{4E} \right) + O(\epsilon^4) .
\end{aligned}$$

We notice that, with the exception of $\nu_\mu \rightarrow \nu_\tau$, the transition probabilities are generically of $O(\epsilon^2)$. In the 3+1 scheme, on the contrary,

$$\begin{aligned}
P_{CP}^{3+1}(\nu_e \rightarrow \nu_\mu) &= P_{CP}^{3+1}(\nu_e \rightarrow \nu_\tau) = P_{CP}^{3+1}(\nu_\mu \rightarrow \nu_\tau) = O(\epsilon^4) , \\
P_{CP}^{3+1}(\nu_\mu \rightarrow \nu_\mu) &= P_{CP}^{3+1}(\nu_e \rightarrow \nu_e) = 1 - 4\epsilon^2 \sin^2 \left(\frac{\Delta m_{34}^2 L}{4E} \right) + O(\epsilon^4) ;
\end{aligned}$$

all the appearance transition probabilities are generically of $O(\epsilon^4)$. This explains the (slight) decrease in the sensitivity in the 3+1 scheme with respect to the 2+2 scheme. The 2+2 $\nu_\mu \rightarrow \nu_\tau$ case is similar to the generic situation in the 3+1 scheme: Fig. 6 and Fig. 9 (right) show the same sensitivity reach, indeed.

Finally, we also present the MNS mixing matrix in the two schemes at $O(\epsilon)$:

$$U^{2+2} = \begin{pmatrix} 1 & 0 & \epsilon & \epsilon \\ 0 & 1 & \epsilon e^{i\delta_3} & \epsilon \\ -\epsilon & -\epsilon e^{-i\delta_3} & 1 & 0 \\ -\epsilon & -\epsilon & 0 & 1 \end{pmatrix} + O(\epsilon^2) , \quad (41)$$

$$U^{3+1} = \begin{pmatrix} 1 & 0 & 0 & \epsilon \\ 0 & 1 & 0 & \epsilon \\ 0 & 0 & 1 & \epsilon \\ -\epsilon & -\epsilon & -\epsilon & 1 \end{pmatrix} + O(\epsilon^2) . \quad (42)$$

We remind that in the 2+2 scheme the sterile neutrino is in the first row, $\nu_\alpha = \{\nu_s, \nu_e, \nu_\mu, \nu_\tau\}$, whereas in the 3+1 scheme is in the last one, $\nu_\alpha = \{\nu_e, \nu_\mu, \nu_\tau, \nu_s\}$. We can build the main contributions to the transition probabilities first writing ν_α, ν_β as linear combinations of mass eigenstates with coefficients given in eqs. (41) and (42), and then computing $|\langle \nu_\alpha(t) | \nu_\beta \rangle|^2$. In this way it is simple to derive the behaviour of all the transition probabilities $P(\nu_\alpha \rightarrow \nu_\beta)$.

4 CP-violating Observables

Genuine CP-violating effects manifest only when at least two mass differences are simultaneously non-vanishing. In the three-family model, the CP-violating contribu-

tion to the oscillation probabilities can be written as [55]:

$$P_{CP} = \pm 2J(\sin 2\Delta_{12} + \sin 2\Delta_{23} - \sin 2\Delta_{13}) \quad (43)$$

with $J = c_{12}s_{12}c_{13}^2s_{13}c_{23}s_{23}\sin\delta$ the Jarlskog factor and Δ_{ij} as defined in eq. (3) (the \pm sign refers to neutrinos/antineutrinos). If $\Delta_{12} \ll \Delta_{23}$, P_{CP} is negligible. Therefore, for three-family neutrino mixing the size of the CP-violating oscillation probability depends on the range of Δm_{12}^2 , the solar mass difference. In [32, 33] it has been shown that a maximal phase, $|\delta| = 90^\circ$, can be measured at 90% CL if the LMA-MSW solution with $\Delta m_{12}^2 \geq 2 \times 10^{-5}$ eV² is considered. For smaller values of the solar mass difference, it seems impossible to measure δ with the foreseeable beams. However, in the four-family model the situation is totally different [56]: we can consider CP-violating observables that do not depend on Δ_{sol} , but on Δ_{atm} and Δ_{LSND} only. Therefore, for four-family neutrino mixing, large CP-violating effects are possible (depending on the specific value of the phases δ_i). In the two-mass dominance approximation the parameter space consists of five rotation angles and two phases, both for the 2+2 and 3+1 schemes. In the 2+2 scheme, the CP-violating oscillation probabilities are given by eqs. (11-13). We notice that, in these expressions, the size of the CP-violating probability is linearly dependent on the atmospheric mass difference, Δ_{34} , whereas the location of the maximum depends on the LSND mass difference, Δ_{23} . Therefore, we expect a maximum in the CP-violating observable at $O(10)$ Km for neutrinos of $E_\nu = O(10)$ GeV. With such a short baseline, matter effects are completely negligible. In the 3+1 scheme, eqs. (21-23), similar results are obtained for $\Delta_{atm} = \Delta_{23}$ and $\Delta_{LSND} = \Delta_{34}$. This has to be compared with the three-family model, where the size of the CP-violating probability depends linearly on Δ_{sol} and the maximum location depends on Δ_{atm} : in this case, the maximum of the CP-observable is expected at $O(1000)$ Km, and therefore matter effects are extremely important [57].

CP-odd effects are observable in appearance channels, while disappearance ones are only sensitive to the CP-even part. The easiest way to measure CP-violation in oscillation is to build a CP-asymmetry or a T-asymmetry [29]:

$$A_{\alpha\beta}^{CP} \equiv \frac{P(\nu_\alpha \rightarrow \nu_\beta) - P(\bar{\nu}_\alpha \rightarrow \bar{\nu}_\beta)}{P(\nu_\alpha \rightarrow \nu_\beta) + P(\bar{\nu}_\alpha \rightarrow \bar{\nu}_\beta)}, \quad (44)$$

$$A_{\alpha\beta}^T \equiv \frac{P(\nu_\alpha \rightarrow \nu_\beta) - P(\nu_\beta \rightarrow \nu_\alpha)}{P(\nu_\alpha \rightarrow \nu_\beta) + P(\nu_\beta \rightarrow \nu_\alpha)}. \quad (45)$$

$A_{\alpha\beta}^{CP}$ and $A_{\alpha\beta}^T$ are theoretically equivalent in vacuum due to *CPT*, and matter effects are negligible at the short distances under consideration. Their extraction from data at a Neutrino factory is quite different, though. Consider, as an example, the $(\nu_e \rightarrow \nu_\mu)$ channel. The CP-asymmetry, $A_{e\mu}^{CP}$, would be measured by first extracting $P(\nu_e \rightarrow \nu_\mu)$ from the produced (wrong-sign) μ^- s in a beam from μ^+ decay and $P(\bar{\nu}_e \rightarrow \bar{\nu}_\mu)$ from the charge conjugate beam and process. Notice that even if the fluxes are very well known, this requires a good knowledge of the cross section ratio $\sigma(\bar{\nu}_\mu \rightarrow \mu^+)/\sigma(\nu_\mu \rightarrow \mu^-)$. Conversely, the measurement of the T-asymmetry, $A_{e\mu}^T$, requires to consider $P(\nu_\mu \rightarrow$

ν_e) and thus a good e charge identification, that seems harder to achieve from the experimental point of view. In the following we will deal only with CP-asymmetries.

A central question on the observability of CP-violation is that of statistics. We do not exploit here the explicit E_ν dependence of the CP-odd effect, and we consider the neutrino-energy integrated quantity:

$$\bar{A}_{\alpha\beta}^{CP}(\delta) = \frac{\{N[l_\beta^-]/N_o[l_\alpha^-]\}_+ - \{N[l_\beta^+]/N_o[l_\alpha^+]\}_-}{\{N[l_\beta^-]/N_o[l_\alpha^-]\}_+ + \{N[l_\beta^+]/N_o[l_\alpha^+]\}_-}, \quad (46)$$

where l_α, l_β are the charged leptons produced via CC interactions by ν_α, ν_β , respectively (the sign of the decaying muons is indicated by an upper index). $N[l_\beta^\pm]$ is the number of CC interactions due to oscillated neutrinos, whereas $N_o[l_\alpha^\pm]$ is the expected number of CC interactions in the absence of oscillations. In order to quantify the significance of the signal, we compare the value of the integrated asymmetry with its error, $\Delta\bar{A}_{\alpha\beta}^{CP}$, in which we include the statistical error and a conservative background estimate at the level of 10^{-5} .

In what follows we used the exact expression for the oscillation probabilities, thus including the small Δ_{sol} mass difference and the matter effects. The irrelevance of the latter at the considered baseline can be seen in Fig. 10, where $\bar{A}_{e\mu}^{CP}(\delta = 90^\circ)/\Delta\bar{A}_{e\mu}^{CP}$ in the 3+1 scheme is presented: we see that matter effects start to be relevant at $O(1000)$ Km.

Since the matter effects are negligible, the scaling laws with the muon energy E_μ and the baseline L of the signal-to-noise ratio of the CP-violating asymmetry in eq. (46) are equivalent to those obtained in vacuum,

$$\frac{\bar{A}_{\alpha\beta}^{CP}}{\Delta\bar{A}_{\alpha\beta}^{CP}} \propto \sqrt{E_\nu} \left| \sin \left(\frac{\Delta m_{LSND}^2 L}{4E_\nu} \right) \right|. \quad (47)$$

4.1 CP-violation in the 2+2 scheme

We recall here the results of [35, 36], albeit rederived with slightly different input parameters. In the conservative assumption of small gap-crossing angles, $\theta_{13}, \theta_{14}, \theta_{23}$ and θ_{24} , we consider the following values for the parameters of the MNS mixing matrix in the two-mass dominance approximation:

$$\begin{aligned} \theta_{13} &= \theta_{14} = \theta_{23} = \theta_{24} = 2^\circ; \theta_{12} = 45^\circ, \theta_{34} = 45^\circ; \\ \Delta m_{12}^2 &= 10^{-4} \text{ eV}^2, \Delta m_{34}^2 = 3.5 \times 10^{-3} \text{ eV}^2, \Delta m_{23}^2 = 1 \text{ eV}^2; \\ A &= 1.1 \times 10^{-4} \frac{\text{eV}^2}{\text{GeV}}. \end{aligned} \quad (48)$$

The detector characteristics have been given in Sect. 2.2.

- **Integrated asymmetry in the $\nu_e \rightarrow \nu_\mu$ channel**

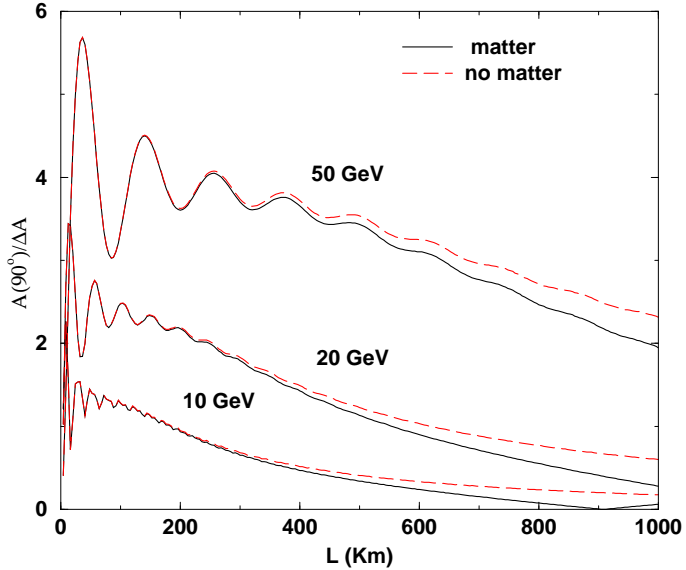


Figure 10: *Signal-to-noise ratio of the CP-violating asymmetry in the $\nu_e \rightarrow \nu_\mu$ channel with and without matter effects, for $E_\mu = 10, 20$ and 50 GeV, as a function of the baseline L . The parameters are: $\Delta m_{sol}^2 = 10^{-4}$ eV 2 ; $\Delta m_{atm}^2 = 3.5 \times 10^{-3}$ eV 2 ; $\Delta m_{LSND}^2 = 1$ eV 2 ; $\theta_{12} = 22.5^\circ$, $\theta_{13} = 13^\circ$, $\theta_{23} = 45^\circ$; $\theta_{14} = \theta_{24} = \theta_{34} = 5^\circ$; $\delta_2 = 0^\circ$, $\delta_3 = 90^\circ$. The matter parameter, $A = 2E_\nu \sqrt{2}G_F n_e$ (with n_e the electron density in the Earth) is taken to be constant, $A = 1.1 \times 10^{-4}$ eV 2 / GeV. This value is consistent with a baseline completely contained in the Earth crust [58], true for $L \leq 4000$ Km.*

In Fig. 11 we show the signal-to-noise ratio of the integrated CP asymmetry, eq. (46), in the $\nu_e \rightarrow \nu_\mu$ channel, as a function of the distance L for three values of the parent muon energy, $E_\mu = 10, 20$ and 50 GeV. Matter effects, although negligible, are included. For this reason, we subtract to the total asymmetry $\bar{A}_{e\mu}^{CP}(90^\circ)$ the matter-induced asymmetry, $\bar{A}_{e\mu}^{CP}(0^\circ)$. We notice that a sizeable signal can be reached: for $E_\mu = 50$ GeV, approximately 10 standard deviations (sd) at $L \simeq 30$ Km can be attained. The scaling of the maximum height with the parent muon energy follows eq. (47) as expected, increasing with $\sqrt{E_\mu}$.

- **Integrated asymmetry in the $\nu_e \rightarrow \nu_\tau$ channel**

In Fig. 12 we show the signal-to-noise ratio of the subtracted integrated CP asymmetry in the $\nu_e \rightarrow \nu_\tau$ channel. The results are pretty similar to those for the $\nu_e \rightarrow \nu_\mu$ channel, with a slightly smaller significance at the maximum: for $E_\mu = 50$ GeV, ~ 8 sd can be attained at $L \simeq 30$ Km.

- **Integrated asymmetry in the $\nu_\mu \rightarrow \nu_\tau$ channel**

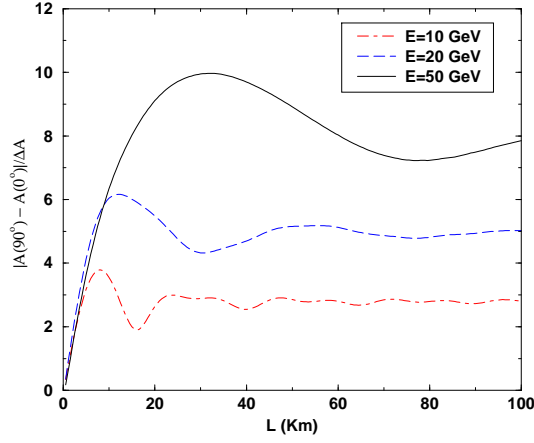


Figure 11: *Signal over statistical uncertainty for CP violation in the $\nu_e \rightarrow \nu_\mu$ channel in the 2+2 scheme, as a function of the baseline L , for three values of the parent muon energy, $E_\mu = 10, 20$ and 50 GeV. The parameters have been chosen as in eq. (48), with $\delta_2 = 0^\circ, \delta_3 = 90^\circ$.*

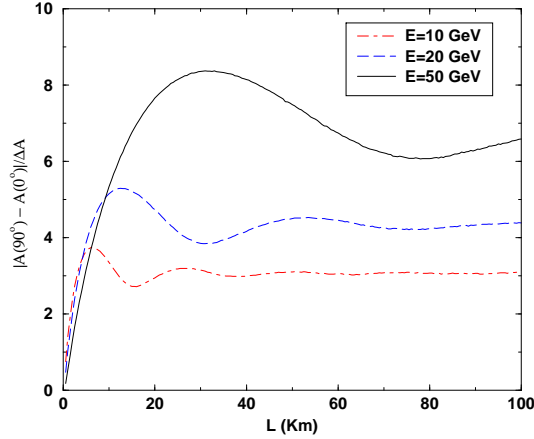


Figure 12: *Signal over statistical uncertainty for CP violation in the $\nu_e \rightarrow \nu_\tau$ channel in the 2+2 scheme, as a function of the baseline L , for three values of the parent muon energy, $E_\mu = 10, 20$ and 50 GeV. The parameters have been chosen as in eq. (48), with $\delta_2 = 0^\circ, \delta_3 = 90^\circ$.*

In Fig. 13 we show the signal-to-noise ratio of the subtracted integrated CP asymmetry in the $\nu_\mu \rightarrow \nu_\tau$ channel. The results are totally different from those relative to $\nu_e \rightarrow \nu_\mu, \nu_\tau$: for $E_\mu = 50$ GeV, ~ 90 sd can be attained at $L \simeq 30$ Km.

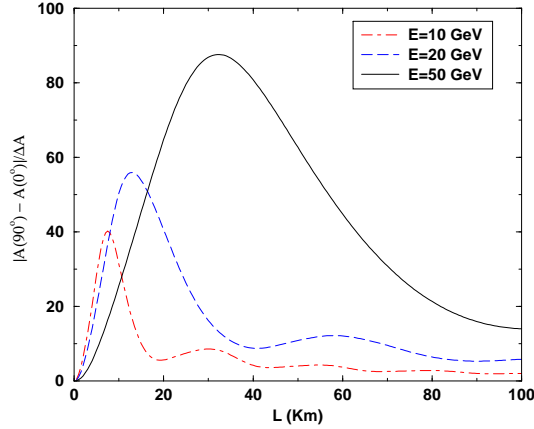


Figure 13: *Signal over statistical uncertainty for CP violation in the $\nu_\mu \rightarrow \nu_\tau$ channel in the 2+2 scheme, as a function of the baseline L , for three values of the parent muon energy, $E_\mu = 10, 20$ and 50 GeV. The parameters have been chosen as in eq. (48), with $\delta_2 = 0^\circ, \delta_3 = 90^\circ$.*

4.2 CP-violation in the 3+1 scheme

In the conservative assumption of small gap-crossing angles, θ_{14}, θ_{24} and θ_{34} , we consider the following values for the parameters of the MNS mixing matrix in the two-mass dominance approximation:

$$\begin{aligned} \theta_{14} &= \theta_{24} = \theta_{34} = 2^\circ; \theta_{12} = 22.5^\circ, \theta_{13} = 13^\circ, \theta_{23} = 45^\circ; \\ \Delta m_{12}^2 &= 10^{-4} \text{ eV}^2, \Delta m_{23}^2 = 3.5 \times 10^{-3} \text{ eV}^2, \Delta m_{34}^2 = 1 \text{ eV}^2; \\ A &= 1.1 \times 10^{-4} \frac{\text{eV}^2}{\text{GeV}}. \end{aligned} \quad (49)$$

- **Integrated asymmetry in the $\nu_e \rightarrow \nu_\mu$ channel**

In Fig. 14 we show the signal-to-noise ratio of the subtracted integrated CP asymmetry in the $\nu_e \rightarrow \nu_\mu$ channel, as a function of the distance L for three values of the parent muon energy, $E_\mu = 10, 20$ and 50 GeV. The results are quite similar to those obtained in the 2+2 scheme, although the significance is slightly less: for $E_\mu = 50$ GeV, ~ 6 sd at $L \simeq 40$ Km can be attained.

The most unfortunate case is presented in Fig. 15. We show the signal-to-noise ratio of the subtracted integrated CP asymmetry as a function of the distance L for three values of the CP-violating phases, $\delta_2 = \delta_3 = 15^\circ, 45^\circ$ and 90° . In the 3+1 scheme the corresponding oscillation probability, eq. (21), contains three different terms in $\sin \delta_2$, $\sin \delta_3$ (with opposite signs) and $\sin(\delta_2 - \delta_3)$. Therefore, when $\delta_2 = \delta_3$ a cancellation occurs. This is the reason of the decrease in the significance for $\delta_2 = \delta_3 = 90^\circ$ with

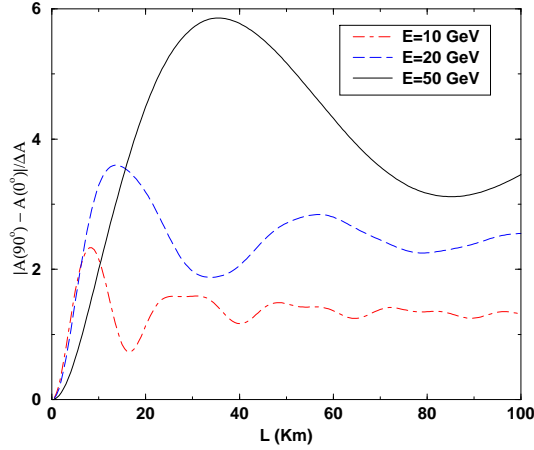


Figure 14: *Signal over statistical uncertainty for CP violation in the $\nu_e \rightarrow \nu_\mu$ channel in the 3+1 scheme, as a function of the baseline L , for three values of the parent muon energy, $E_\mu = 10, 20$ and 50 GeV. The parameters have been chosen as in eq. (49), with $\delta_2 = 0^\circ, \delta_3 = 90^\circ$.*

respect to the corresponding curve in Fig. 14. For the lowest value of the phase only ~ 0.02 sd can be attained.

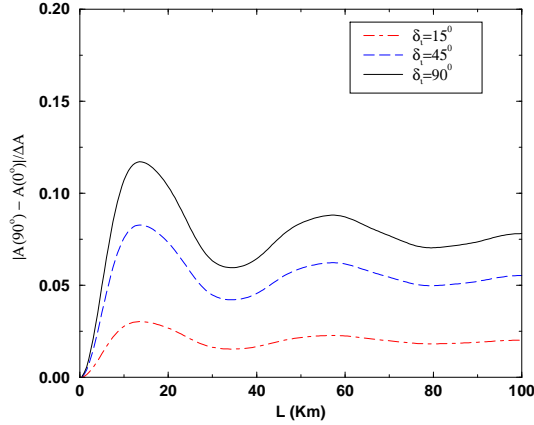


Figure 15: *Signal over statistical uncertainty for CP violation in the $\nu_e \rightarrow \nu_\mu$ channel in the 3+1 scheme, as a function of the baseline L , for three values of the phases, $\delta_2 = \delta_3 = 15^\circ, 45^\circ$ and 90° . The parameters have been chosen as in eq. (49), with $E_\mu = 20$ GeV.*

- **Integrated asymmetry in the $\nu_e \rightarrow \nu_\tau$ channel**

In Fig. 16 we show the signal-to-noise ratio of the subtracted integrated CP asymmetry in the $\nu_e \rightarrow \nu_\tau$ channel. The results are pretty similar to those for the $\nu_e \rightarrow \nu_\mu$ channel, with a slightly smaller significance at the maximum: for $E_\mu = 50$ GeV, ~ 5 sd can be attained at $L \simeq 40$ Km.

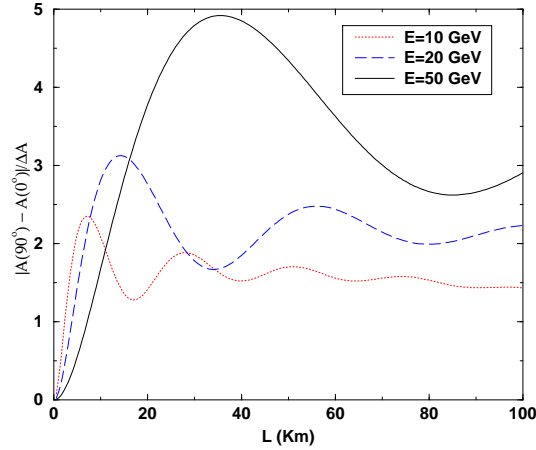


Figure 16: *Signal over statistical uncertainty for CP violation in the $\nu_e \rightarrow \nu_\tau$ channel in the 3+1 scheme, as a function of the baseline L , for three values of the parent muon energy, $E_\mu = 10, 20$ and 50 GeV. The parameters have been chosen as in eq. (49), with $\delta_2 = 0^\circ, \delta_3 = 90^\circ$.*

- **Integrated asymmetry in the $\nu_\mu \rightarrow \nu_\tau$ channel**

In Fig. 17 we show the signal-to-noise ratio of the subtracted integrated CP asymmetry in the $\nu_\mu \rightarrow \nu_\tau$ channel. Again, as in the 2+2 scheme, the results are totally different from those relative to $\nu_e \rightarrow \nu_\mu, \nu_\tau$. For $E_\mu = 50$ GeV, ~ 100 sd can be attained at $L \simeq 40$ Km.

In Fig. 18 we show the signal-to-noise ratio of the subtracted integrated CP asymmetry as a function of the distance L for three values of the CP-violating phases, $\delta_2 = \delta_3 = 15^\circ, 45^\circ$ and 90° . The oscillation probability at the leading order only depends on $\sin \delta_2$, see eq. (23). In this case, for the lowest value of the phase ~ 10 sd can still be reached.

4.3 Remarks and conclusions on the CP-violation observables

The previous results clearly show how a maximal CP-violation is easily measurable with a not-so-large detector of 10 Kton size, at a baseline $L = O(10)$ Km. The optimal

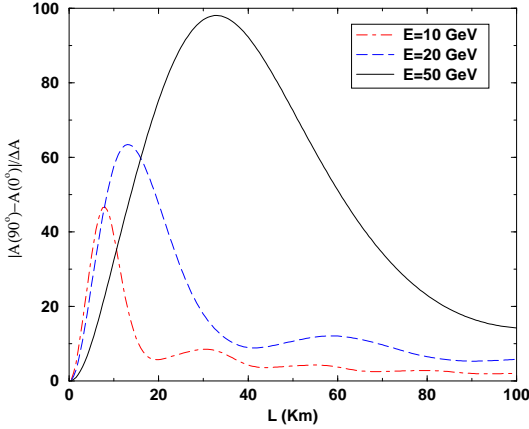


Figure 17: *Signal over statistical uncertainty for CP violation in the $\nu_\mu \rightarrow \nu_\tau$ channel in the 3+1 scheme, as a function of the baseline L , for three values of the parent muon energy, $E_\mu = 10, 20$ and 50 GeV. The parameters have been chosen as in eq. (49), with $\delta_2 = 90^\circ, \delta_3 = 0^\circ$.*

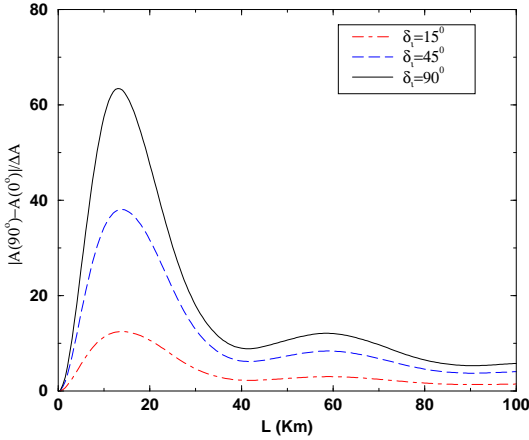


Figure 18: *Signal over statistical uncertainty for CP violation in the $\nu_\mu \rightarrow \nu_\tau$ channel in the 3+1 scheme, as a function of the baseline L , for three values of the phases, $\delta_2 = \delta_3 = 15^\circ, 45^\circ$ and 90° . The parameters have been chosen as in eq. (49), with $E_\mu = 20$ GeV.*

channel to observe CP-violation is the $\nu_\mu \rightarrow \nu_\tau$ channel, where $O(100)$ sd can be attained. Even at lower energies, $\sim 40 - 50$ sd can be easily found. The number of expected N_{τ^\pm} in the detector is of $O(10^5)$. Notice that in the $\nu_\mu \rightarrow \nu_\tau$ channel a non-maximal CP-violating phase gives a significance at the level of ~ 10 sd even for the lowest energy, $E_\mu = 10$ GeV. The other two channels, $\nu_e \rightarrow \nu_\mu, \nu_\tau$ are quite similar and give much smaller significance. For a smaller detector mass M , a reduction

factor $\propto 1/\sqrt{M}$ should be applied to all the results of this section. Therefore, for an OPERA-like 1 Kton detector we still expect large CP-violating effects in the $\nu_\mu \rightarrow \nu_\tau$ channel.

All of these results are obtained in both the 2+2 and the 3+1 scheme, with slight differences between the two. The real gain with respect to the three-family model is that the small solar mass difference, that modulates the overall size of the CP-violating asymmetry, is traded with the much larger atmospheric mass difference.

In the three-family model, the largest CP asymmetry is expected in the $\nu_e \rightarrow \nu_\mu$ transition. We have shown that in the four-family model (both in the 2+2 and 3+1 scheme) this is not the case: it is $\nu_\mu \rightarrow \nu_\tau$ the optimal channel to study CP violation. The reason can be easily understood applying the power counting argument introduced in Sect. 3.3. Neglecting the background, the signal-to-noise ratio of the CP asymmetry $A_{\alpha\beta}^{CP}/\Delta A_{\alpha\beta}^{CP}$ is:

$$\frac{A_{\alpha\beta}^{CP}}{\Delta A_{\alpha\beta}^{CP}} \propto \frac{P_{CP}(\nu_\alpha \rightarrow \nu_\beta)}{\sqrt{P_{CP}(\nu_\alpha \rightarrow \nu_\beta)}} \quad (50)$$

The CP-violating transition probabilities in the approximation of equally small gap-crossing angles, $\sin \theta_{ij} \simeq \epsilon$ (with θ_{ij} a generic gap-crossing angle in the 2+2 or the 3+1 scheme), in the 2+2 scheme become:

$$P_{CP}^{2+2}(\nu_e \rightarrow \nu_\mu) = -4\epsilon^2 \sin(2\theta_{34}) \sin(\delta_2 + \delta_3) \left(\frac{\Delta m_{34}^2 L}{4E_\nu} \right) \sin^2 \left(\frac{\Delta m_{23}^2 L}{4E_\nu} \right) + O(\epsilon^4), \quad (51)$$

$$P_{CP}^{2+2}(\nu_e \rightarrow \nu_\tau) = +4\epsilon^2 \sin(2\theta_{34}) \sin(\delta_2 + \delta_3) \left(\frac{\Delta m_{34}^2 L}{4E_\nu} \right) \sin^2 \left(\frac{\Delta m_{23}^2 L}{4E_\nu} \right) + O(\epsilon^4), \quad (52)$$

$$P_{CP}^{2+2}(\nu_\mu \rightarrow \nu_\tau) = -4\epsilon^2 \sin(2\theta_{34}) [\sin \delta_2 + \sin(\delta_2 + \delta_3)] \left(\frac{\Delta m_{34}^2 L}{4E_\nu} \right) \sin^2 \left(\frac{\Delta m_{23}^2 L}{4E_\nu} \right) + O(\epsilon^4); \quad (53)$$

in the 3+1 scheme become:

$$P_{CP}^{3+1}(\nu_e \rightarrow \nu_\mu) = 4\epsilon^3 \sin(2\theta_{23}) \sin(\delta_2 - \delta_3) \left(\frac{\Delta m_{23}^2 L}{4E_\nu} \right) \sin^2 \left(\frac{\Delta m_{34}^2 L}{4E_\nu} \right) + O(\epsilon^4), \quad (54)$$

$$P_{CP}^{3+1}(\nu_e \rightarrow \nu_\tau) = -8\epsilon^3 c_{23}^2 \sin \delta_3 \left(\frac{\Delta m_{23}^2 L}{4E_\nu} \right) \sin^2 \left(\frac{\Delta m_{34}^2 L}{4E_\nu} \right) + O(\epsilon^4), \quad (55)$$

$$P_{CP}^{3+1}(\nu_\mu \rightarrow \nu_\tau) = -4\epsilon^2 \sin(2\theta_{23}) \sin \delta_2 \left(\frac{\Delta m_{23}^2 L}{4E_\nu} \right) \sin^2 \left(\frac{\Delta m_{34}^2 L}{4E_\nu} \right) + O(\epsilon^4) \quad (56)$$

Scheme	Transition	P_{CP}	P_{CP}	$A/\Delta A$
Three-family	$\nu_e \rightarrow \nu_\mu$	ϵ^2	ϵ	$O(1)$
	$\nu_e \rightarrow \nu_\tau$	ϵ^2	ϵ	$O(1)$
	$\nu_\mu \rightarrow \nu_\tau$	1	ϵ	$O(\epsilon)$
2+2	$\nu_e \rightarrow \nu_\mu$	ϵ^2	ϵ^2	$O(\epsilon)$
	$\nu_e \rightarrow \nu_\tau$	ϵ^2	ϵ^2	$O(\epsilon)$
	$\nu_\mu \rightarrow \nu_\tau$	ϵ^4	ϵ^2	$O(1)$
3+1	$\nu_e \rightarrow \nu_\mu$	ϵ^4	ϵ^3	$O(\epsilon)$
	$\nu_e \rightarrow \nu_\tau$	ϵ^4	ϵ^3	$O(\epsilon)$
	$\nu_\mu \rightarrow \nu_\tau$	ϵ^4	ϵ^2	$O(1)$

Table 3: *Small angles suppression in the CP-conserving and CP-violating oscillation probabilities, and in the signal-to-noise ratio of the CP asymmetries, in the three-family model and in both four-family model mass schemes.*

(in this case we have considered $s_{13} \sim \epsilon$ also, since the present experimental results in the three-family model show that $\theta_{13} \leq 13^\circ$ [54]).

In Tab. 3 we report the leading order in ϵ for the different P_{CP} and P_{CP} in the three-family model and in both schemes of the four-family model. In three-family, the small parameter is $s_{13} \sim \epsilon$. In four-family we consider equally small LSND gap-crossing angles: $s_{13} = s_{14} = s_{23} = s_{24} \sim \epsilon$ for the 2+2 scheme; $s_{14} = s_{24} = s_{34} = \epsilon$ for the 3+1 scheme. In this last case we take $s_{13} \sim \epsilon$, also. We also report the leading order in ϵ of the signal-to-noise ratio of the various CP asymmetries, using eq. (50).

The last column can be easily read: in the three-family model, the $\nu_e \rightarrow \nu_\mu$ and $\nu_e \rightarrow \nu_\tau$ have a signal-to-noise ratio of the corresponding CP asymmetry of $O(1)$ in the small angles. On the contrary, in both the 2+2 and 3+1 four-family model, it is the $\nu_\mu \rightarrow \nu_\tau$ channel to be of $O(1)$ in the small angles, thus justifying *a posteriori* our results. As a final remark, notice that the last column for the 2+2 and the 3+1 scheme is identical, although the corresponding CP-conserving and CP-violating probabilities are of different order in the small angles suppression.

5 A magnetized iron detector with no τ -tracking

In this section we explore the possibility of reconstructing two angles or one angle and a phase at a time in a short baseline experiment, $L = 40$ Km (the distance where the CP-violating observable of the previous section is maximized). We focus on the $\nu_e \rightarrow \nu_\mu$ channel and consider a realistic 10 Kton magnetized iron detector with μ charge identification of the type discussed in [37]. A detailed analysis of the backgrounds and detection efficiencies of this apparatus can be found in the literature. The Neutrino

Factory is run with 2×10^{20} useful muons per year for 5 operational years for both muon polarities at $E_\mu = 50$ GeV, with a detector energy resolution of $\Delta E_\nu = 10$ GeV. Our motivation is the following: is it possible to avoid the complications connected with the τ detection taking full advantage of the energy dependence in the $\nu_e \rightarrow \nu_\mu$ channel, instead?

We follow the procedure described in [32]: let $N_{i,p}$ be the total number of wrong-sign muons detected when the Neutrino Factory is run in polarity $p = \mu^+, \mu^-$, grouped in 5 energy bins specified by $i = 1$ to 5. In order to simulate a typical experimental situation we generate a set of “data” $n_{i,p}$ as follows: for a given value of the oscillation parameters, the expected number of events, $N_{i,p}$, is computed; taking into account backgrounds and detection efficiencies per bin, $b_{i,p}$ and $\epsilon_{i,p}$ (as quoted in [32]), we perform a Gaussian (or Poisson, depending on the number of events) smearing to mimic the statistical uncertainty:

$$n_{i,p} = \frac{\text{Smear}(N_{i,p}\epsilon_{i,p} + b_{i,p}) - b_{i,p}}{\epsilon_{i,p}}. \quad (57)$$

The “data” are then fitted to the theoretical expectation as a function of the mixing matrix parameters under study, using a χ^2 minimization:

$$\chi^2 = \sum_p \sum_i \left(\frac{n_{i,p} - N_{i,p}}{\delta n_{i,p}} \right)^2, \quad (58)$$

where $\delta n_{i,p}$ is the error on $n_{i,p}$ (we include no error in the efficiencies).

First consider the simultaneous measurement of θ_{14} and θ_{24} . In the one-mass dominance approximation the $\nu_e \rightarrow \nu_\mu$ transition probability, eq. (16), depends on the combination $s_{14}^2 s_{24}^2$. This term (symmetric under $\theta_{14} \leftrightarrow \theta_{24}$) dominates over the sub-leading Δm_{atm}^2 -dependent (non-symmetric) corrections. Therefore, the energy dependence of $N_{i,p}$ is not enough to resolve the two angles.

Next, we consider the simultaneous measurement of θ_{34} and one of θ_{14}, θ_{24} . We compute the leading corrections to eq. (16) in powers of Δm_{atm}^2 . For vanishing phases and $s_{13} = s_{24} = \epsilon$, $\theta_{23} = 45^\circ$, the leading terms are

$$\begin{aligned} P_{CP}^{3+1}(\nu_e \rightarrow \nu_\mu) &= 4\epsilon^2 s_{14}^2 c_{34}^4 \sin^2 \Delta_{34} - 2c_{34}^2 s_{34} s_{14}^2 \epsilon \Delta_{23} \sin(2\Delta_{34}) \\ &+ O(\epsilon^4) + O(\Delta_{23}^2) + O(\epsilon^2 \Delta_{23}). \end{aligned} \quad (59)$$

For vanishing phases and $s_{13} = s_{14} = \epsilon$, $\theta_{23} = 45^\circ$, the leading terms are, instead,

$$P_{CP}^{3+1}(\nu_e \rightarrow \nu_\mu) = 4\epsilon^2 c_{24}^2 s_{24}^2 c_{34}^4 \sin^2 \Delta_{34} + O(\epsilon^4) + O(\Delta_{23}^2) + O(\epsilon^2 \Delta_{23}). \quad (60)$$

In Fig. 19 (left) we present the 68, 90 and 99 % confidence level contours for a simultaneous fit of θ_{14} and θ_{34} for a “data” set generated with $\theta_{14} = 5^\circ$, $\theta_{24} = 2^\circ$ and $\theta_{34} = 6^\circ$. This figure corresponds to eq. (59), where the leading correction to the one-mass dominance formula is $O(\epsilon \Delta_{23})$. In Fig. 19 (right) we present the 68, 90 and 99 %

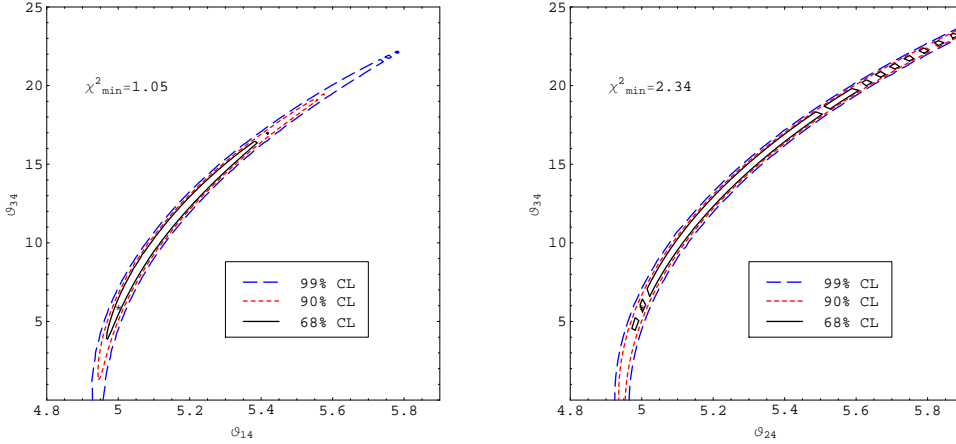


Figure 19: 68, 90 and 99 % CL contours resulting from a χ^2 fit of θ_{14} and θ_{34} (left) or θ_{24} and θ_{34} (right). The parameters used to generate the “data” are depicted by a star: $\theta_{14} = 5^\circ, \theta_{34} = 6^\circ$ (left); $\theta_{24} = 5^\circ, \theta_{34} = 6^\circ$ (right). Only statistical errors are included.

confidence level contours for a simultaneous fit of θ_{24} and θ_{34} for a “data” set generated with $\theta_{24} = 5^\circ, \theta_{14} = 2^\circ$ and $\theta_{34} = 6^\circ$. This figure corresponds to eq. (60): notice that the $O(\epsilon\Delta_{23})$ correction to the one-mass dominance formula is absent and the leading corrections start at higher orders. The sensitivity to θ_{34} is therefore suppressed with respect to eq. (59). In summary, θ_{14} or θ_{24} are reconstructed with a precision of tenths of degree; on the contrary, θ_{34} is measurable with a very poor precision in both cases, with slightly better results in Fig. 19 (left).

We try also to simultaneously fit the combination $s_{14}s_{24}$ and θ_{34} . In Fig. 20 we generate the “data” for $s_{14}s_{24} = 0.09, \theta_{34} = 5^\circ$. As in Fig. 19, we observe that θ_{34} is poorly reconstructed, whereas $s_{14}s_{24}$ is severely constrained. Our results seem to indicate that is very difficult to measure θ_{34} using the energy dependence of sub-leading effects in the $\nu_e \rightarrow \nu_\mu$ channel.

Finally, we consider the simultaneous measurement of one gap-crossing angles (the other two being fixed at some small value) and one CP-violating phase. In this case, the leading correction to the one-mass dominance formula, eq. (16), is the CP-odd contribution, eq. (21). In Fig. 21 we show the confidence level contours for a simultaneous fit of θ_{14} and δ_3 . The theoretical values for which the “experimental data” have been generated are: $\theta_{14} = 3^\circ, \delta_3 = 50^\circ$ ($\theta_{24} = \theta_{34} = 2^\circ$). We see that the angle is reconstructed with a precision of tenths of degree, whereas the phase is measured with a precision of tens of degrees only. This is precisely the same situation of the three-family results of [32], however.

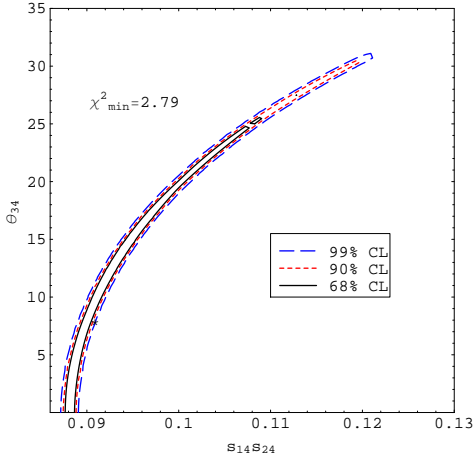


Figure 20: 68, 90 and 99 % CL contours resulting from a χ^2 fit of $s_{14}s_{24}$ and θ_{34} . The parameters used to generate the “data” are depicted by a star, $s_{14}s_{24} = 0.09, \theta_{34} = 5^\circ$. Only statistical errors are included.

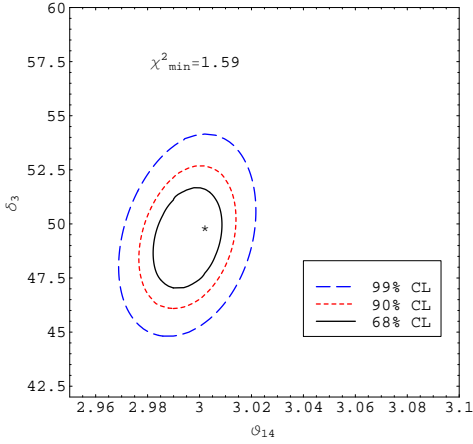


Figure 21: 68, 90 and 99 % CL contours resulting from a χ^2 fit of θ_{14} and δ_3 (left). The parameters used to generate the “data” are depicted by a star, $\theta_{14} = 3^\circ, \delta_3 = 50^\circ$. Only statistical errors are included.

6 Conclusions

The ensemble of solar, atmospheric and LSND neutrino data can be explained with three active plus one sterile flavour states. Although the four-family neutrino mass spectrum preferred by the experimental data is the so-called 2+2 scheme (with two almost degenerate pairs well separated by the LSND mass difference), the latest LSND

result are marginally (at 99 % CL) compatible with the 3+1 scheme (three almost degenerate neutrinos separated from a fourth, mainly sterile, one).

In this paper we studied the physical potential of a Neutrino Factory in both four-family model schemes, in the spirit of [35, 36] where the 2+2 scheme was carefully examined. A re-analysis of the 2+2 results and a totally novel analysis in the 3+1 scheme has been presented. We have derived one- and two-mass scale dominance approximations appropriate for CP-even and CP-odd observables, respectively, in both schemes.

The rich flavour content of a muon-decay based beam is extremely useful to determine or severely constrain the four-family model parameter space: in both schemes, the sensitivity to gap-crossing angles as small as $\sin^2 \theta_{ij} = 10^{-6} - 10^{-4}$ (depending on the specific angle) can be achieved, with a 1 ton detector at $L \sim 1$ Km down from the source, for $n_\mu = 2 \times 10^{20}$ useful muons per year and 5 years of data taking. In the 3+1 scheme, we notice a slight loss in sensitivity with respect to the 2+2 scheme, that we interpret as a consequence of the higher power in the small gap-crossing angles in the leading terms of the CP-conserving transition probabilities.

CP violation may be easily at reach with a 10 Kton detector at $L = O(10)$ Km, especially through “ τ appearance” signals, in both schemes. The increased significance of the CP-violating observables with respect to the three-family model asymmetries is due to the fact that asymmetries proportional to Δm_{atm}^2 are possible, whereas in the three-family model the CP-violating asymmetries are proportional to the small Δm_{sol}^2 . Moreover, in the four-family case the asymmetries are modulated by Δm_{LSND}^2 , thus peaking at $L = O(10)$ Km; in three families they are modulated by Δm_{atm}^2 and therefore they peak at $L = O(1000)$ Km, thus significantly suffering from matter effects. On the contrary, matter effects are totally negligible in the four-family case. We give a simple argument based again on the power counting of the small gap-crossing mixing angle to explain why in four-family models (both in the 2+2 and 3+1 schemes) the $\nu_\mu \rightarrow \nu_\tau$ channel is the optimal one to study CP-violating observables, whereas in three families $\nu_e \rightarrow \nu_\mu$ seems to be best suited.

Eventually, we consider a 10 Kton detector at $L = 40$ Km with only μ charge identification (of the magnetized iron type). In this case, we use the energy dependence of the wrong-sign muons to try to simultaneously reconstruct two angles (or combinations of them) or a CP-violating phase and one angle at a time. Our results suggest that it is not possible to constrain the whole CP-conserving parameter space using the $\nu_e \rightarrow \nu_\mu$ channel only. However, we can simultaneously measure one angle and one phase, with a precision of tens of degrees in the latter.

Summarizing, a Neutrino Factory has an enormous discovery potential when four-neutrino models are considered, in both the 2+2 and 3+1 schemes. If the LSND results will be confirmed by MiniBooNE, a muon storage ring appears to be an extremely powerful facility to perform precision measurement on the whole four-family model parameter space and most probably the best opportunity to discover CP violation

in the leptonic sector. A (not-so-large) detector with τ -tracking and (μ, τ) charge identification capability is needed. If MiniBooNE will not confirm LSND, however, the 3+1 scheme will still represent a possible extension of the Standard Model and a Neutrino Factory can severely constrain its parameter space. This cannot be said of the 2+2 scheme, that would be ruled out by a negative result of MiniBooNE.

Acknowledgements

We acknowledge useful conversations with M.B. Gavela, J.J. Gomez Cadenas, P. Hernandez, P. Lipari and S. Rigolin. We are particularly indebted with M. Lusignoli for discussions on many different aspects of this paper.

References

- [1] B. T. Cleveland *et al.*, *Astrophys. J.* **496** (1998) 505.
- [2] Y. Fukuda *et al.* [Kamiokande Collaboration], *Phys. Rev. Lett.* **77** (1996) 1683.
- [3] W. Hampel *et al.* [GALLEX Collaboration], *Phys. Lett.* **B447** (1999) 127.
- [4] J. N. Abdurashitov *et al.* [SAGE Collaboration], *Phys. Rev.* **C60** (1999) 055801.
- [5] Y. Suzuki [Super-Kamiokande Collaboration], *Nucl. Phys. Proc. Suppl.* **77** (1999) 35.
- [6] Y. Fukuda *et al.* [Kamiokande Collaboration], *Phys. Lett.* **B335** (1994) 237.
- [7] R. Becker-Szendy *et al.*, *Nucl. Phys. Proc. Suppl.* **38** (1995) 331.
- [8] Y. Fukuda *et al.* [SuperKamiokande Collaboration], *Phys. Rev. Lett.* **82** (1999) 2644.
- [9] W. W. Allison *et al.* [Soudan-2 Collaboration], *Phys. Lett.* **B449** (1999) 137.
- [10] M. Ambrosio *et al.* [MACRO Collaboration], *Phys. Lett.* **B434** (1998) 451.
- [11] T. Toshito, talk at the XXXVI Rencontres de Moriond, 10-17 March 2001, Les Arcs, France.
- [12] C. Athanassopoulos *et al.* [LSND Collaboration], *Phys. Rev. Lett.* **81** (1998) 1774.
- [13] A. Aguilar [LSND Collaboration], hep-ex/0104049.
- [14] E. Church *et al.* [BooNe Collaboration], nucl-ex/9706011.

- [15] B. Pontecorvo, Sov. Phys. JETP **26** (1968) 984.
- [16] C. Caso *et al.*, EPJ **C3** (1998), 319.
- [17] G. L. Fogli, E. Lisi, A. Marrone and G. Scioscia, hep-ph/9906450.
- [18] S. M. Bilenkii *et al.*, Phys. Rev. **D60** (1999) 073007.
- [19] G. Mills, talk at Neutrino 2000, 16-21 June 2000, Sudbury, Canada.
- [20] F. Dydak *et al.*, Phys. Lett. B **134** (1984) 281.
- [21] I. E. Stockdale *et al.*, Z. Phys. C **27** (1985) 53.
- [22] Y. Declais *et al.*, Nucl. Phys. **B434** (1995) 503.
- [23] W. Grimus and T. Schwetz, hep-ph/0102252.
- [24] V. Barger, B. Kayser, J. Learned, T. Weiler and K. Whisnant, Phys. Lett. B **489** (2000) 345 [hep-ph/0008019].
- [25] C. Giunti and M. Laveder, JHEP **0102** (2001) 001 [hep-ph/0010009].
- [26] O. L. Peres and A. Y. Smirnov, Nucl. Phys. B **599** (2001) 3 [hep-ph/0011054].
- [27] O. Yasuda, hep-ph/0007076.
- [28] S. Geer, Phys. Rev. D **57** (1998) 6989 [Erratum-ibid. D **59** (1998) 039903] [hep-ph/9712290].
- [29] A. De Rujula, M. B. Gavela and P. Hernandez, Nucl. Phys. **B547** (1999) 21.
- [30] C. Albright *et al.*, hep-ex/0008064.
- [31] A. Blondel *et al.*, Nucl. Instrum. Meth. A **451** (2000) 102.
- [32] A. Cervera *et al.*, Nucl. Phys. **B579** (2000) 17.
- [33] A. Cervera *et al.*, hep-ph/0007281.
- [34] J. Burguet-Castell, M. B. Gavela, J. J. Gomez-Cadenas, P. Hernandez and O. Mena, hep-ph/0103258.
- [35] A. Donini *et al.*, Nucl. Phys. **574** (2000) 23.
- [36] A. Donini, M. B. Gavela, P. Hernandez and S. Rigolin, Nucl. Instrum. Meth. A **451** (2000) 58 [hep-ph/9910516].
- [37] A. Cervera, F. Dydak and J. Gomez Cadenas, Nucl. Instrum. Meth. A **451** (2000) 123.

- [38] H. Minakata and H. Nunokawa, Phys. Lett. B **495** (2000) 369 [hep-ph/0004114].
- [39] M. Koike, T. Ota and J. Sato, hep-ph/0011387.
- [40] C. Giunti, M. C. Gonzalez-Garcia and C. Pena-Garay, Phys. Rev. D **62** (2000) 013005 [hep-ph/0001101].
- [41] O. Yasuda, hep-ph/0006319.
- [42] P. Lipari and M. Lusignoli, Phys. Rev. D **58** (1998) 073005 [hep-ph/9803440].
- [43] T. Kajita, talk at NOW 2000, 12-19 September 2000, Otranto, Italia.
- [44] Y. Suzuki, talk at NuFact'00, 22-26 May 2000, Monterey, U.S.A.
- [45] G. L. Fogli, E. Lisi and A. Marrone, Phys. Rev. D **63** (2001) 053008 [hep-ph/0009299].
- [46] Z. Maki, M. Nakagawa and S. Sakata, Prog. Theor. Phys. **28** (1962) 870.
- [47] S. M. Bilenky, S. Pascoli and S. T. Petcov, Neutrinoless Double Beta-Decay: II. Mixing of Four Neutrinos," hep-ph/0104218.
- [48] A. De Rujula, M. Lusignoli, L. Maiani, S. T. Petcov and R. Petronzio, Nucl. Phys. B **168** (1980) 54.
- [49] M. Apollonio *et al.*, Phys. Lett. **B466** (1999) 415.
- [50] J. Kleinfeller [KARMEN Collaboration], Nucl. Phys. Proc. Suppl. **87** (2000) 281.
- [51] T. K. Gaisser, Cosmic Rays and Particle Physics, Cambridge University Press, 1990.
- [52] G. J. Feldman and R. D. Cousins, Phys. Rev. D **57** (1998) 3873 [physics/9711021].
- [53] A. Donini *et al.*, hep-ph/0007283.
- [54] G. L. Fogli, E. Lisi, A. Marrone and G. Scioscia, hep-ph/9904465.
- [55] P. I. Krastev and S. T. Petcov, Phys. Lett. **B205** (1988) 84.
- [56] A. Donini, Nucl. Phys. Proc. Suppl. **100** (2001) 210 [hep-ph/0012153].
- [57] M. Freund *et al.*, Nucl. Phys. **B578** (2000) 27.
- [58] A. M. Dziewonski and D.L. Anderson, Phys. Earth Planet. Int. **25** (1981) 297.